Scientific Research Publishing

Advances in Aerospace Science and Technology, 2022, 7, 52-84
https://www.scirp.org/journal/aast
ISSN Online: 2473-6724
ISSN Print: 2473-6708

Validation of Novel Model for Identification of Thermal Conditions in the Low Corona

Daniel B. Berdichevsky[1,2], Jenny M. Rodríguez Gómez[3,4], Luis E. Vieira[5], Alisson Dal Lago[5]

[1]College Park, Maryland, USA
[2]IFIR/UNR-CONICET, Rosario, Argentina
[3]The Catholic University of America, Washington D.C., USA
[4]NASA Goddard Space Flight Center, Greenbelt, Maryland, USA
[5]Instituto Nacional de Pesquisas Espaciais, INPE, São José dos Campos, Brazil
Email: dbberdi@gmail.com, daniel.b.berdichevsky@nasa.gov, rodriguezgomez@cua.edu, jenny.m.rodriguezgomez@nasa.gov

How to cite this paper: Berdichevsky, D.B., Gómez, J.M.R., Vieira, L.E. and Lago, A.D. (2022) Validation of Novel Model for Identification of Thermal Conditions in the Low Corona. *Advances in Aerospace Science and Technology*, **7**, 52-84.
https://doi.org/10.4236/aast.2022.71004

Received: January 29, 2022
Accepted: March 25, 2022
Published: March 28, 2022

Abstract

The electron density and temperature key properties of the neutral-magnetized plasma in the solar corona, which are predicted with a novel model, provide an interesting window along the whole solar cycle. In this work, we test the quantitative validity of the model and prove that the Coronal Density and Temperature (CODET) is reliable. Furthermore, this work contrasts the CODET model results with alternative observational remote and *in-situ* datasets during the simplest conditions of the quiescent corona near the solar minimum. This successful outcome/validation of the CODET model allowed a good qualitative density and temperature retrieval in the solar corona covering a large portion of time interval from solar cycles 23 and 24.

Keywords

Solar Corona, Electron Density, Temperature

1. Introduction

The solar magnetic field is understood to drive many phenomena in the solar atmosphere. Its relationship with plasma is essential to obtain electron density (N_e) and temperature (T_e) in different time scales. The evidence for magnetic control of the Sun's corona is very large. From observations of the coronal plasma, it is possible to have a picture of the magnetic fields emerging from beneath the Sun's photosphere control essentially all aspects of coronal structure, dynamics, and plasma heating mechanisms through to coronal evolution (Judge, 1998) [1].

Rodríguez Gómez *et al.* (2018) [2] show that the Solar Corona responds to the

influence of the magnetic field below the Solar Corona. Indeed, it appears that the magnetic field contributes fundamentally to most phenomena in the solar atmosphere. Furthermore, we notice that the recent work by Morgan and Taroyan (2017) [3] using a similar global irradiance analysis of the Sun corona through the solar cycle from the year 2010 to the year 2017 than the present approach (see also Rodríguez Gómez, 2017 [4]). This approach uses the Differential Emission Model (DEM) and the scaling laws which describe the temperature in the Solar Coronal. However, the work by Rodríguez Gómez (see, e.g., Rodríguez Gómez (2017) [4], Rodríguez Gómez *et al.* (2018) [2]) covers a more extensive time interval (1995 - 2017) starting from the same basis of the magnetic field on the photosphere and employing comparable techniques to generate mean global changes. However, it differentiates for further giving estimates of electrons density and temperature assuming a Corona in hydromagnetic equilibrium (see below **Figure 1**), showing an example that the assumptions made by Rodríguez Gómez allow recovery variations in a large time scale.

Notice that total solar eclipses provide a unique view of the Solar Corona, allowing us to explore the electron density, temperature, and general thermodynamics

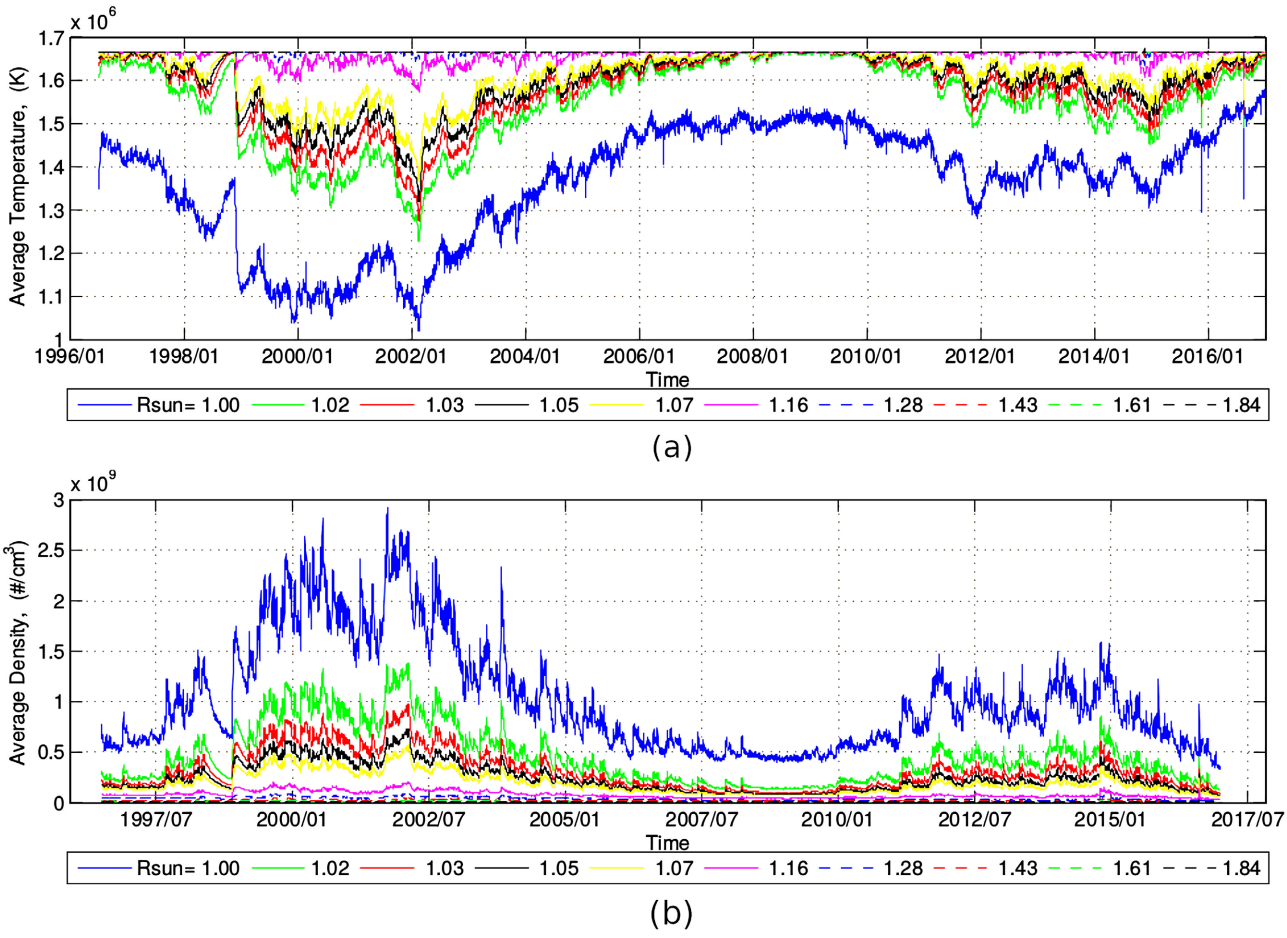

Figure 1. View of the low corona dependence on the altitude of electrons T_e (a) and N_e (b) from the CODET model and their progression in time covering cycle 23 and most of cycle 24.

of the solar corona (Aschwanden (2019) [5]). However, these are rare events, and it is necessary to use models to obtain estimations on a large time scale, e.g., the CODET model. Therefore, the purpose of this study is to present a quantitative description of the T_e and N_e of the low corona for a new CODET model parameter-set. Furthermore, we proceed to put the new parameter set for the model under a thorough quality check.

In this work, we performance a CODET model validation on Quiet Sun solar minimum from Jan. 1, 2008, to Jan. 1, 2009. Following the next steps:

- We used the CODET model to obtain density, temperature, average magnetic energy density, magnetic pressure, and kinetic pressure;
- Check the consistency of density and temperature estimates with remote sensing solar corona observations, *i.e.*, coronagraph images, EUV images from EIT/SOHO instrument, and 1 AU *in-situ* solar wind observations;
- The temperature of the low solar corona from the width of the iron non-thermal lines was evaluated using solar irradiance.

Section 2 revisits the method to obtain the CODET model parameters based on radiance observations. Section 3 is devoted to checking the remote most careful identifications of the conditions of the Solar Corona in the essential properties of the temperature and plasma density, with the help of Coronagraph remote plasma density identifications and magnetic field measurements at 1 AU. Finally, Section 4 focuses on the global manifestations of the low corona, and conclusions are drawn in Section 5.

2. Review of the COronal DEnsity and Temperature (CODET) Model

The relationship between plasma and the solar magnetic field is briefly reviewed here. The CODET model was recently developed to obtain electron density and temperature estimations in the solar atmosphere and the results are surprisingly accurate in a qualitative representation over 15 years of continuous observation of the solar corona. The CODET model using a set of parameters allows estimated density and temperature in the solar corona during solar cycles 23 and 24. It offered an exciting opportunity to analyze the thermodynamic conditions in quailtatively of the solar corona during an extended fraction of the duration of both recently past solar cycles. Furthermore, it offers an interesting opportunity to analyze the thermodynamics of the solar corona during the last two solar cycles. The new recent results on densities and temperature obtained from the CODET model are encouraging. Here, we validate the overall simple qualitative description of the low corona by Rodríguez Gómez *et al.* (2017) [2] and (2018) [4]. We proceed in this work to check the quality of their quantitative adjustment of the model parameters to the more straightforward stage of the scenario of the Solar Minimum, in this way checking its very quality of description of the low Corona in its quiescent times-interval.

The quite simple description of T_e, N_e, shown in **Figure 1**, constitutes a global

view of their evolution along the solar cycle, and a few other observables are derived using a method introduced recently, see Rodríguez Gómez *et al.* (2018) [2]. Specifically, we concern ourselves here with the Coronal Density and Temperature (CODET) model's success in its qualitative description of the K-corona over more than 11 years, *i.e.*, more than a solar cycle. Although, N_e and T_e can be inferred from remote sensing images of the inner corona, and *in-situ* measurements in the interplanetary medium. When these models are effective, e.g., Rodríguez Gómez (2017) [4], require further understanding of the underlying physics. In this work we attempt to fill the gap for the simplest case scenario, *i.e.*, the quiescent solar corona. In this scenario we attempt to present a quantitative estimate and compare it to the best observational capability to reproduce T_e and N_e.

Figure 1 shows that Rodríguez Gómez (2017) [4] allows recovery variations on a large time scale. We describe the CODET model and the main results for a solar cycle interval near its minimum (one year). These are the electron (e)-number and temperature profiles in three specific layers through the solar corona in a region limited between $1.1R_\odot$ and $1.3R_\odot$. The CODET model is designed for a quantitative description of the corona and here we validate it for a solar minimum period, the long-lasting solar minimum starting in 2008 and extending in the time until the end of the year 2009. In Section 3, we combine remote solar corona observations from a variety of instruments of SOHO, details from the total solar eclipse from August 1, 2008 and earlier solar eclipse studies, and *in-situ* SW observations lasting several Carrington rotations to constraint the possibilities of the kind of solar corona to which we will apply our assumptions of its thermal properties, as they are derived from the global model (CODET) which provide the very good qualitative description as seen in **Figure 1**, for an interval that extends from the solar minimum which connects solar cycles 22 and 23 up to passing the solar maximum of solar cycle 24. Also, the magnetic and kinetic pressure in this period, indication of the presence of ARs is further explored in the corona with the help of EUV images from EIT/SOHO. Finally, we add a consideration that allows us to neglect the impact of equatorial Coronal Holes (CHs) present during extended intervals of the solar minimum considered.

The CODET model uses magnetic field data provided by MDI/SOHO (Scherrer *et al.* (1995) [6]) and HMI/SDO (Scherrer *et al.* (2012) [7]). The Potential Field Source Surface (PFSS) was used to obtain the structure of the coronal magnetic field from $1R_\odot$ to $2.5R_\odot$ (Schrijver (2001) [8]; Schrijver & De Rosa (2003) [9]). We used a model based on Chianti atomic database 8.0 (Del Zanna *et al.* (2015) [10]). The emission model describes the characteristics of the EUV produced lines; 17.1 nm (FeIX), 19.3 nm (FeXII), and 21.1 nm (FeXIV). The optimization algorithm Pikaia (Charbonneau (1995) [11]) was used to research for the best fit-parameters, which adequately describe the density and temperature profiles through the solar atmosphere (**Figure 1**). We use BELUGA that is a MATLAB optimization package and is freely available from Medical School at University

of Michigan in the virtual physiological Rat Project[1]. Beluga finds in a local minimum x of an objective function (CODET model) an initial population of possible solutions. The goodness-of-fit between the observed and modelling data, in general was $\chi^2 \leq 1$ indicates an acceptable fit.

The optimization algorithm plays an important role in the CODET model because it is the key to the connection between observed and modeled irradiance (**Figure 2**). Various tests to find the goodness of fit between modeled and observational irradiance were made using individual and multiple wavelengths simultaneously, *i.e.*, find the goodness of fit between observational and modeled irradiance at 17.1 nm, 19.3 nm, and 21.1 nm (individually) and using these three wavelengths simultaneously (more details see Rodríguez Gómez J.M. (2017) [4]).

The goodness-of-fit allows us to make inferences about observed values or compare these values with modeled ones. The Chi-square (χ^2) test is one quantitative criterion for a good fit. In general, suppose we measure N quantities to obtain the experimental values x_i with standard errors σ_i. We also have theoretical expressions for these quantities. These expressions contain a set of n parameters a_m whose values are adjusted to give the best fit to the data. A theoretical expression for x_i can be written as $\xi_i = \xi_i(a_1, a_2, ..., a_n)$. We can consider the case where the probability distributions for the experimental results x_i are Gaussian. Then the likelihood function is proportional to:

$$L(a_1, a_2, \mathrm{L}\ , a_n) = \frac{1}{(2\pi)^{N/2}\sigma_1\sigma_2\mathrm{L}} \mathrm{e}^{-\left(\sum_{i=1}^{N}\frac{(x_i-\xi_i)^2}{2\sigma_i^2}\right)} \tag{1.a}$$

to adjust the parameters a_m and give a maximum likelihood, it is equivalent to minimizing the exponent:

$$\sum_{i=1}^{N}\frac{(x_i-\xi_i)^2}{2\sigma_i^2} = \frac{1}{2}\chi^2(a_m) \tag{1.b}$$

Equation (1.b) is called a least-squares fit. This expression allows defining the Chi-square (χ^2) test. It consists of deciding whether the exponent in the likelihood

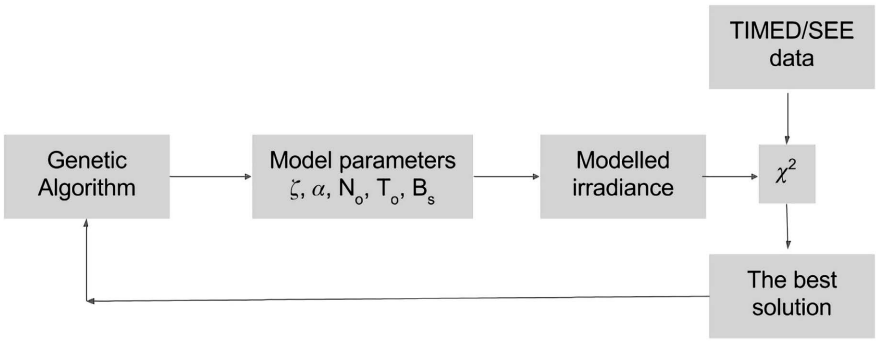

Figure 2. Flow diagram of the process involved in the generation of the CODET model as developed recently, see Rodríguez Gómez (2017) [4].

[1]http://virtualrat.org/software/beluga

function is larger than one should expect statistically (Mathews & Walker (1970) [12]). Several cases were explored to search for the best fit between the observational data and data from the CODET model, including the usual definition of the Chi-square (χ^2) test described above Equations (1.a) and (1.b). These descriptions could not find the best fit because three different wavelengths were fitted simultaneously (17.1 nm, 19.3 nm, and 21.1 nm). Thus, to obtain the goodness-of-fit between modeled and TIMED/SEE irradiance data, we proceeded to perform the Chi-square test described below. χ^2 function was defined as:

$$\chi^2 = \frac{\left(I_{model} - I_{obs}\right)^2}{\left|I_{obs}\right|} \tag{1.c}$$

where I_{obs} correspond to the irradiance measured by TIMED/SEE, and I_{model} is the modeled irradiance in all wavelengths (17.1 nm, 19.3 nm, and 21.1 nm). The goodness of the fit is defined by:

$$\chi^2 = \chi^2_{17.1\text{nm}} + \chi^2_{19.3\text{nm}} + \chi^2_{21.1\text{nm}} \tag{1.d}$$

In this case, the goodness of fit is for $\chi^2 = 0.0010$. This value was reached with the model parameters presented in **Table 1**. It should be noted that our fitting scheme departs from the standard χ^2 *-test* definition in the forcing to be zero the non-diagonal optimization matrix terms (see e.g., Mathews and Walker (1970) [12]) between the different wavelength adjustments performed simultaneously for 17.1 nm, 19.3 nm, and 21.1 nm, which we expressed in the manner of Equation (1.d).

Table 1. Constants and the parameters of the model.

Parameter	Value	Model	Reference
$B\left(\frac{r}{R_e}\right)$ for $r > R_e$	Model evaluation	PFSS[a] input to SFTM[b] Instrument/Dataset SOHO/MDI, SDO/HMI	Aschwanden/ Schatten/ Schrijver
R_e	7×10^5 km	Standard value	Photosphere distance to Sun center
R_{Bth0}	$1.2R_\odot$	CODET[c]	Rodríguez Gómez, 2017
B_{Bth0}	3.7700 G	CODET	Rodríguez Gómez, 2017
B_{sat}	4.1750 G	CODET	Rodríguez Gómez, 2017
ξ	1.2520	CODET-new parameters	This work
N_o	2.9500×10^8 e/cm^3	CODET-new parameters	This work
α	−1.4938	CODET-new parameters	This work
T_o	1.6600×10^6 K	CODET-new parameters	This work
$f_t(\text{cadence})$	1/24hrs	CODET	Rodríguez Gómez, 2017

[a]PFSS = Potential Field Source Surface model, see Altshuler and Newkirk, 1969 [17]; [b]SFTM = Surface Flux Transport Model of photosphere magnetism, developed by Schrijver, 2001 [8]; [c]CODET = Integrated model in Rodríguez Gómez, 2017 [4]. This model uses as input the extrapolated radial magnetic field through the solar atmosphere from the PFSS model, and the magnetic flux transport model SFTM. It is shown that conservation of magnetic flux is assumed in the model.

Nevertheless, this approach showed a better model parameters optimization than the more commonly found in the standard statistics books χ^2-fit definition (for more details, see Rodríguez Gómez (2017) [4]). These model parameters, also listed in **Table 1**, were then used to derive electrons gas temperature and the number of particles per cm^3 for the interval of interest, the quiescent Sun corona at extended solar minimum, concentrating our analysis in the second part of year 2008.

In this approach, the scaling laws allow a description of the electron gas density and temperature profiles. For this purpose, we employed density and temperature as a function of the magnetic field (see, e.g., Robbrecht *et al.* (2010) [13]; Yokoyama and Shibata (2001) [14]; Golub (1983) [15]; Emslie (1985) [16]). On this occasion, an extremely Quiet Sun corona, the description does not use the loop length of each magnetic field line. Instead, we show the main results related to density, temperature, magnetic energy, magnetic and kinetic pressure. A small interval is considered from Jan. 1, 2008 to Jan. 1, 2009. For these quiescent solar conditions, **Figure 3** and **Figure 4** show a year's description of the electron gas temperature and density (see **Figure 3**) dependence with altitude to the photosphere. The model parameters used are listed in **Table 1**, and the scaling law relationships, including equations and illustrative Figures showing changes as a function of height, are outlined in the following Subsections 2.1 and 2.2.

2.1. The Model Parameters Used in the Quiet Solar Minimum

The quiet solar minimum model parameters used are listed in **Table 1**, and the

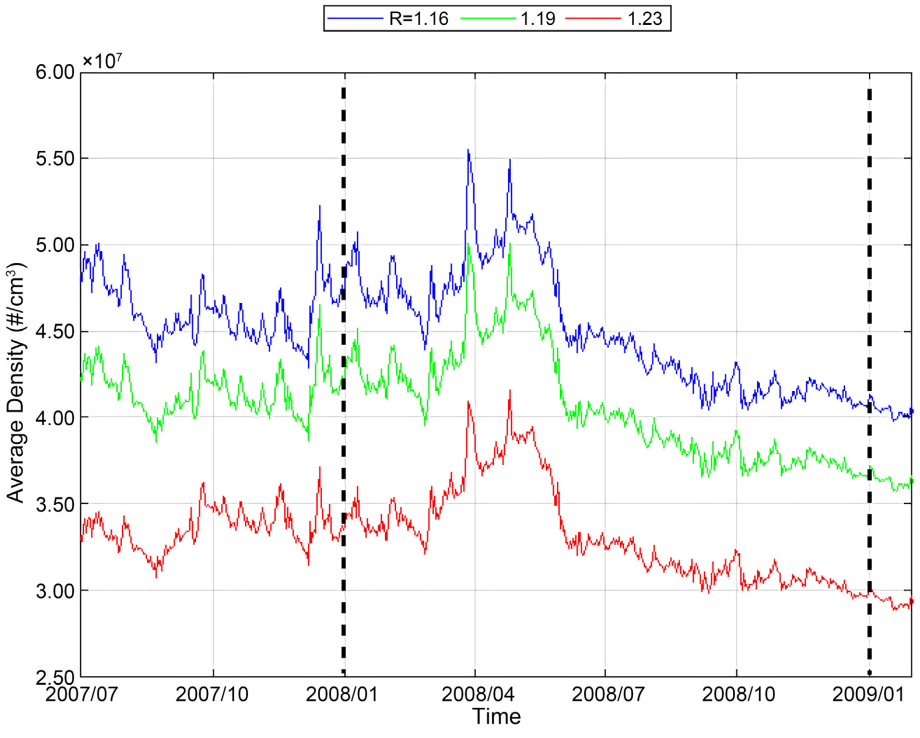

(a)

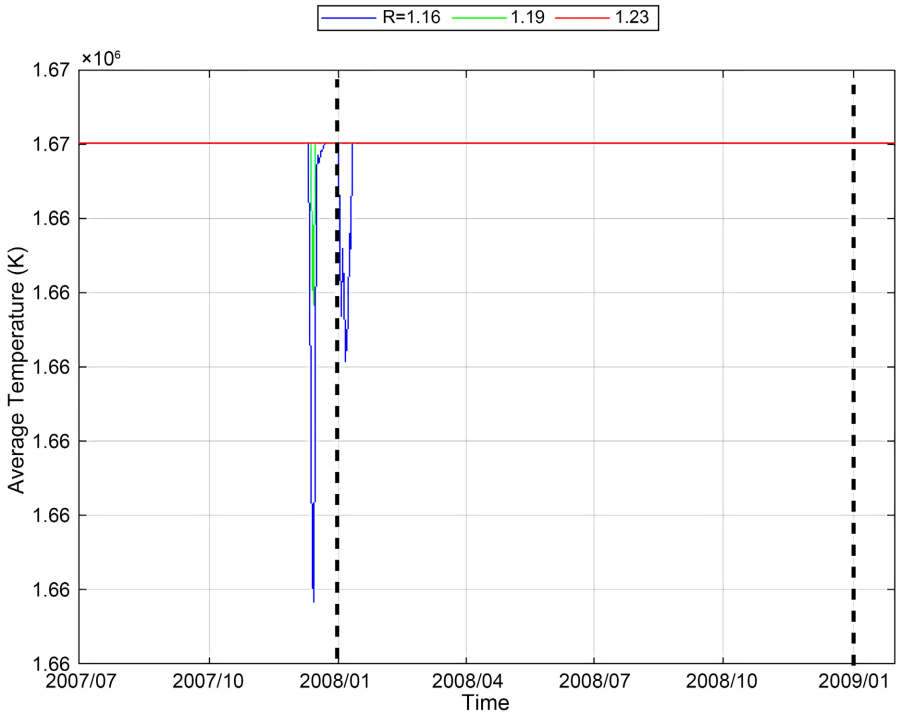

(b)

Figure 3. Density profile N_e the number electrons per cubic cm (a) and temperature profiles (b), the interval of interest in this work extends between dotted vertical lines, from January 1, 2008, to January 1, 2009, at different heights: $1.16R_\odot$ (blue line), $1.19R_\odot$ (green line), $1.23R_\odot$ (red line).

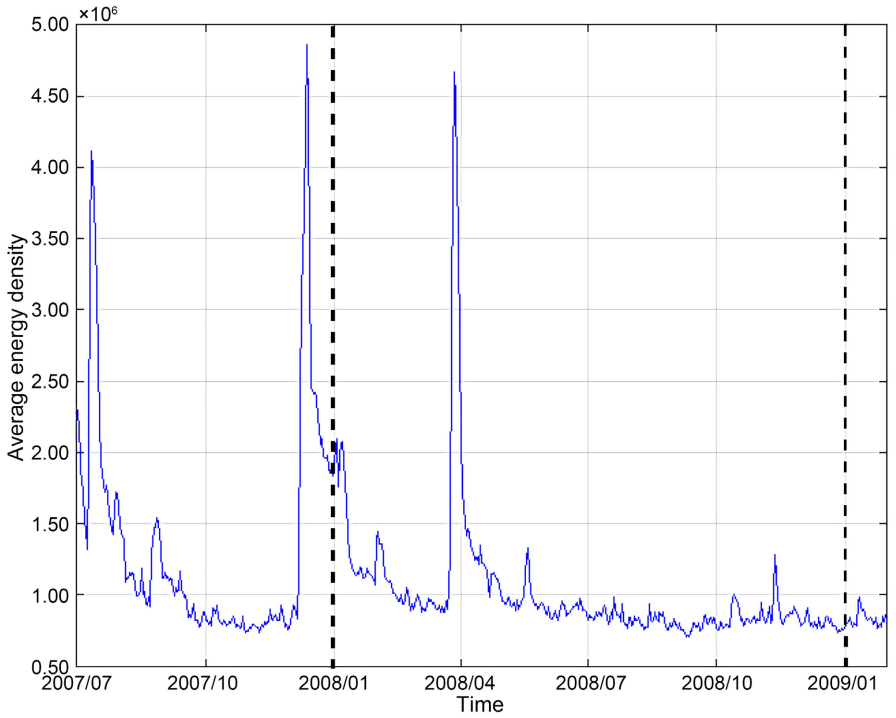

Figure 4. Average magnetic energy density, in ergs per cubic cm, vertical dotted lines demarcate time interval considered.

scaling law relationships, including equations and illustrative figures showing changes as a function of height are outlined in this and the following sections.

2.2. Consistency of CODET Model with Its Irradiance Input Observations

The density profile (Figure 3) is described by the following expression:

$$N = N_o \left(\frac{B}{B_{sat}} \right)^2 \tag{2}$$

where $B_{sat} = 4.17$ Gauss, $N_o = 2.95 \times 10^8$, and $\xi = 1.252$, where ξ is the constant identified as γ in Rodríguez Gómez 2017 [2] and Rodríguez Gómez *et al.* 2018 [4].

The density profile shows an increase from 2008/03 to 2008/06 in all layers (Figure 3). After this period the density decreases in all layers.

The temperature profile definition is:

$$B_{th} = B_{tho} \mathrm{e}^{-(r/R_{bth})^2} \tag{3}$$

where $B_{tho} = 20$ Gauss and $R_{bth} = 1.2R_e$. Using the following conditions, it is possible to define the temperature profile (see Figure 4):

$$\text{If} \quad B < B_{th} \quad T = T_o \tag{4.a}$$

$$\text{And if} \quad B \geq B_{th} \quad T = T_o \left(B / B_{sat} \right)^{\alpha} \tag{4.b}$$

where T_o, B_{sat} and α are listed in Table 1.

The right panel of Figure 3 shows temperature profiles from January 1, 2008, to January 1, 2009. Black vertical dotted lines demarcate the interval discussed in this work. Three different layers were considered $1.16R_\odot$ (blue line), $1.19R_\odot$ (green line), $1.23R_\odot$ (red line). The temperature profiles show variation in 2008/01 (Figure 3, right panel). A decrease from 1.665×10^6 K (at $R = 1.19R_e$ and $R = 1.23R_e$) to 1.6636×10^6 K (at $R = 1.16R_e$) was shown. The internal layer $R = 1.16R_e$ show a lower value than $R = 1.19R_e$ and $R = 1.23R_e$ where the temperature profile is constant, due to the relation with the extrapolated magnetic field. It is important to stress that—after PFSS predictions—the extrapolated magnetic field is near-constant at each altitude in these three "external" layers in the solar corona.

The energy density is calculated using the following expression:

$$nB = \frac{\text{energy}}{\text{volume}} = 1/4\pi \left(B^2 / \mu_o \right) \tag{5}$$

where nB is the energy density, B correspond to the magnetic field from $1R_\odot$ to $2.5R_\odot$ (from PFSS) and μ_o is the magnetic permeability ($4\pi \times 10^{-7}$ kg·m·A^2/s^2) in the vacuum (it corresponds to an assumption in this model). The average energy density is obtained from $1R_\odot$ to $2.5R_\odot$, then the mean value was obtained, to have an estimate in the solar atmosphere.

Figure 4 shows that the magnetic energy density through the solar corona shows an increase near to the 2008/04 and later this energy decrease shows small varia-

tions.

The magnetic energy pressure analysis was done using the magnetic field from PFSS:

$$B = \left(B_r^2 + B_\varphi^2 + B_\theta^2 \right)^{1/2} \tag{6}$$

where B_r, B_φ, B_θ are the magnetic field components from Potential Field Source Surface (PFSS), see e.g., Altschuler and Newkirk, 1969. The magnetic pressure:

$$P_m = B^2 / \left(8\pi\mu_o \right) \tag{7.a}$$

Figure 5 (upper panel) illustrates that the magnetic pressure shows increased values from 2008/03 to 2008/06. The maximum value appears in 2008/04, after that the magnetic pressure presents small variations related to a quiet corona.

The kinetic pressure analysis was made using the following expression:

$$P = \left(N/Vol \right) k_B T \tag{7.b}$$

where N corresponds to the mean electron (e^-) number and T is the e-temperature in each layer. k_B is the Boltzmann constant and Vol is the volume, we consider convenient to use in each layer. Notice that often observations give a direct estimate of the (N/Vol) either in remote or *in-situ* estimates (see values in **Table 1**).

In general terms we can express:

$$Vol = 4\pi r^2 \delta r$$

where r corresponds to the radius in each layer of interest considered $1.16R_\odot$, $1.19R_\odot$ and $1.23R_\odot$.

Figure 5 (right panel) shows that the kinetic pressure presents an increase near 2008/03 whereas after 2008/06 the kinetic pressure decreases. It is related to the average density variations in the same interval. In summary, the description from the CODET model shows a relationship between variations in kinetic pressure, magnetic pressure, electron density, and magnetic energy during the period of interest. The increase of these quantities is correlated among themselves in the period from 2008/03 and 2008/06 and it shows small variations from 2008/07 to 2009/01. In general, the temperature values obtained from these model descriptions are in accord with Osherovich *et al.* 1985 [18]. They describe a relation between magnetic, thermodynamic, and dynamic structures in the solar corona during a sunspot minimum. In the same way, the CODET model assumes magnetic flux tubes in a stratified atmosphere, like the approach in Osherovich 1984 [18]. However, in our approach, the magnetic field decreases with the height in the solar atmosphere. This behavior is due to the description of PFSS B-field lines.

In this section, **Figures 3-5** show the months-long slowly varying, yet under apparently stable conditions, rendered by the observed corona in a variety of light frequencies, e.g., those from the $Fe^{9,12,14}$ ions, suggesting as well as providing.

1) Statistical information on the corona temperature through their ionization temperature.

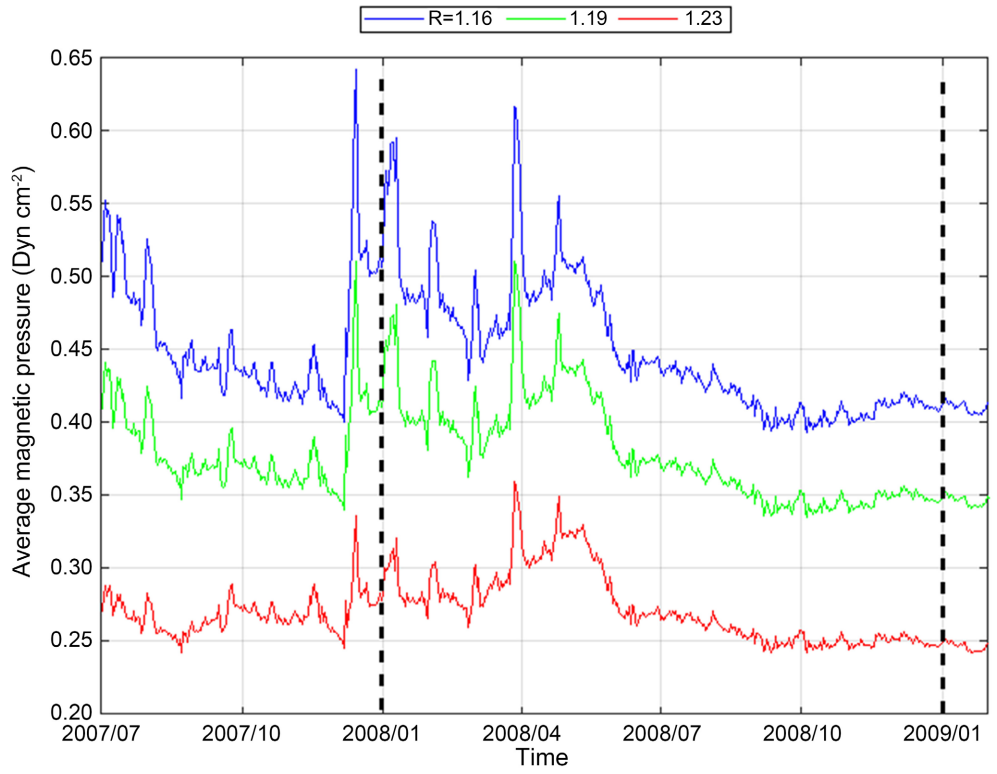

(a)

(b)

Figure 5. Variation in time, at each layer, of the average magnetic pressure (a) and average kinetic pressure (b) through different layers in the solar corona, vertical lines show time intervals.

2) A global state of equilibrium, constituting direct inference of two of several attributes of the quiescent Sun corona near solar minimum. As explained in this section, these observations constrain the choice of the parameters in the successful model of the global values of density and temperature of the electrons in the "low" corona region.

In the next section it is further introduced as an "indirect," central quantity to the modeling. This is the intensity of the magnetic field in the Sun's corona, determined by modeling the magnetic field in the photosphere and inferred through the remote observation of the splitting of the excitation lines of He/O atoms, among other atomic element lines, see e.g., Zirin, 1966 [19].

There is also an interpretation of the manifestation of the magnetic field that is used which assumes it to be the one of an ensemble of flux tubes with an orientation dominated by being horizontal to the solar "sphere."

3. Consistency of Density and Temperature Estimates with Independent Remote Sensing Solar Corona Observations

The optical thin nature of the quiescent Sun corona, see e.g., on the detection of the bending of a far start light, eclipsed by the Sun, see Dyson, Eddington, and Davidson, 1920 [20], makes it difficult to identify the displacement of features, particularly when the density is close to homogeneous, *i.e.*, differs locally in the region of consideration by less than a factor two or even a little greater than that. Check key observables that are mostly located outside of the region of interest guide us toward some of the possible conditions concerning matter and magnetic field in the overall solar corona altitude range studied here. In our case this is a volume contained in the spherical region delimited by $1.1 \leq r/R_{\odot} \leq 1.31$. Our goal is constraining the interpretation of the constitutive nature of the Sun's corona, which enables the CODET model reviewed in Section 2 of global hydromagnetic equilibrium to be quantitatively successful in its predictions. Henceforth, within the limitations of our and other independent solar coronal plasma parameters remote evaluations, we proceed in this section to identify the consistency with them of the CODET model T_e and N_e predictions presented in Section 2.

For the identification of the global properties of interest we take advantage of the observation remotely using: 1) the coronagraph instruments for this and earlier solar minimum from SOHO and STEREO; 2) for the non-thermal light that is measured by the EIT/SOHO instrument (Delaboudinière *et al.* 1995 [21]); and 3) some of its large solar wind manifestations sampled *in-situ* from the Lagrange point L1 between Sun and Earth, with the monitoring of solar wind parameters plasma-protons (Ogilvie *et al.* 1995 [22]), and magnetic field (Lepping *et al.* 1995 [23]), in our case using the Wind SC. We also use Earth's observations of the solar corona during the total eclipse.

During the solar eclipse we explore the magnetic field organization in the quiescent sun corona, from 1.1 to $1.3R_{\odot}$ almost 100% of the source of the radiance, see

Appendix 1, seems to be emission from a hierarchical arrangement of matter, see the imprint of features in **Figure 6(a)** and **Figure 6(b)**. These features, illustrated in **Figure 6(a)** and **Figure 6(b)**, see e.g., Michels, 1998 [24], appear to constitute an ensemble of magnetic flux-tubes oriented mainly parallel to the Sun surface, *i.e.*, photosphere, and see detailed studies of the Sun corona during the occurrence of the total eclipse of the Sun in Voulgaris *et al.* 2010 [25], Habbal *et al.* 2010 [26], Daw *et al.* 2010 [27]. This is then consistent with one of the key assumptions by the CODET model, stated at the end of Section 2.

Although challenging, it is possible to observe the same as all pictures of the Sun presented, **Figure 6** shows cumulated light along the line of sight. In the case of **Figure 6(a)** the observations are captured with the SOHO C1 and C2 near the 1996 solar minimum, see Michels, 1998 [24], for details on the SOHO coronograph observations. Alike, it is possible to observe in the Sun corona, the temporal following of some fraction of arc-sec markers because of their luminosity in a relatively quick succession of coronograph pictures every 12 min in coronal streamers, see e.g., movie of C2/LASCO month of January 1997 and observe changes in small plasma features at about 2 to $3R_{\odot}$ high in the corona (see e.g., Sheeley *et al.* 1997 [28]; Dere, Howard, Brueckner, 2000 [29]). This careful process offers some of the better-delineated examples, *i.e.*, markers suggesting their slow evolution in streamers toward higher and higher altitude becoming at some point the region that constitute a plasma-sheet, a characteristic feature

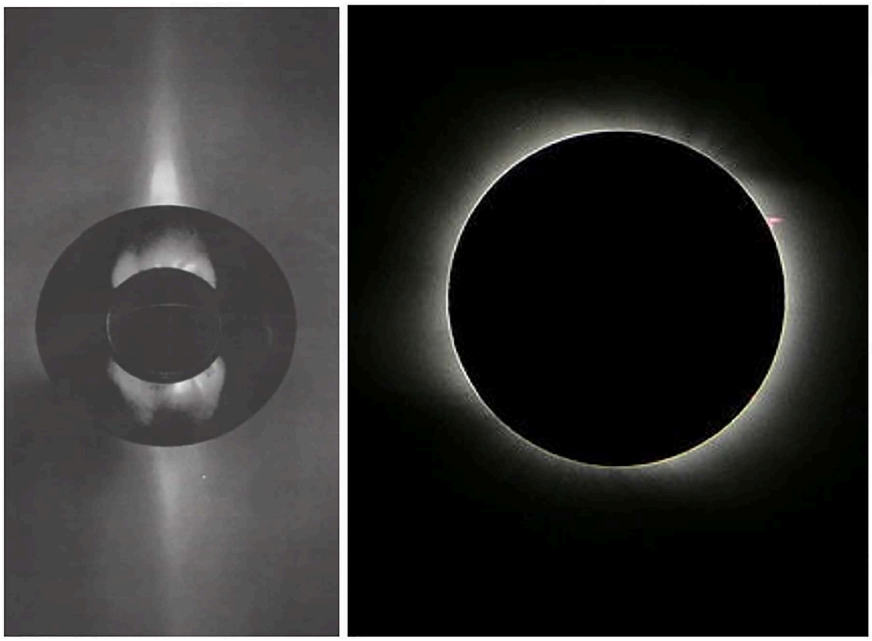

Figure 6. Magnetic field organization in the Solar corona. (a) Near solar minimum from Aug. 1996, the solar plasma sheet self-organization from its beginnings in the low solar corona, starting near $1.1R_{\odot}$ and extending up to $4R_{\odot}$ (Michels D.J. *et al.* 1998 [24]). (b) View of the low solar corona during the total solar eclipse of Aug 1, 2008, region of the corona discussed. The view obtained at Novosibirsk, Russia.

of the nature of the slow to very-slow solar wind (e.g., Vasquez *et al.* 2017 [30]). A contemporary work by Viall and Vourlidas, 2015 [31] says that the start of the SW, related to the quiescent corona in our time interval of interest takes place between 2.0 and 2.5$R_{\odot}$. This SW tends then to possess specific properties when reaching a distance like the location of the orbit of Mercury. A SW that was *in-situ* observed by the two SC of the Helio mission, see e.g., Sanchez-Diaz *et al.* 2016 [32], and which is understood to contain, for most of the time a current sheet in solar minimum that is like a disk surrounding the Sun close to its equatorial region.

In this way, **Figure 6** suggests for larger distances from the Sun, e.g., beyond the one shown in **Figure 6(a)**, and which has been described up to 40 R, a set of contiguous thin equatorial streamers forming a streamer disk, in observations combining the SOHO coronographs C2 and C3 at solar minimum, see e.g., Michels, 1998 [24].

In **Figure 6(a)**, we notice a certain asymmetry in the disk constituting the plasma sheet during the period of the observations presented. A likely cause of that asymmetry is considered below in Subsection 3.3. In consequence it is important to consider that at solar minimum in the Sun corona, there appear the following characteristics:

1) Streamers;

2) Quiescence;

3) Apparent equilibrium;

4) Reduced presence of weak transitory (e.g., flares, filament disappearances) associated or not with sudden ejection of magnetic field and matter that tend to displace at slow speed when compared with the historical mean value of the solar wind convection speed (~400 km·s^{-1}) away from its source, see e.g., [33], Priest, 2014.

A Solar Wind source that is possibly located at about between 2 to 8$R_{\odot}$, depending on the solar corona conditions, see e.g., Schwenn and Marsch, 1990 [34], and ≈2$R_{\odot}$ following SECHI/STEREO observations at solar minimum of interest Viall and Vourlidas, 2015 [31]. Notice that SC Solar Probe perihelia is planned to be to close as 8$R_{\odot}$ in/near 2024.

3.1. Signatures of the EUV Light

During the time interval known as solar minimum, the time when the quiescent sun corona appears to dominate we quote "…the extreme ultraviolet EUV light, monitored to high resolution by the EIT instrument in SOHO shows the reduction in features other than the super-granular well-known arrangement of the Sun's photosphere which contains the rising energy toward the chromosphere and beyond, possibly represented in the form of spicules, rich in the magnetic field and neutral as well as plasma matter from below the photosphere region," see De Pontieu *et al.* 2009 [35], 2011 [36]. Gomez, Bejarano, Mininni, 2014 [37] present an interesting view of magnetized, fully ionized plasma conditions that

we assume may prevail in spicules type II delivering magnetized-matter at/above the chromosphere/corona Transition Region (TR) heights.

In this subsection, we check some features of the solar corona and their evolution during the solar minimum. In this case, we used the EIT/SOHO images in the EUV band, The usual corrections were applied under solarsoft, *i.e.*, EIT images in 19.5 nm, 17.1 nm and 30.4 nm were selected on April 01 (2008), about 14 months away from solar minimum (Figure 7). It is possible to see three ARs (NOAA 10987, 10988 and 10989). The solar corona evolution is illustrated next with about a year to the solar minimum of selected pictures and starting on Jun. 01 (2008). Here we show four images in EIT lines (in Figure 8). It is possible to observe that besides a super-granular network, still, a few features like small AR appear present. The presence of these structures seems somehow reduced at about 6 months from the solar minimum when a whole set of 4 EIT line images are

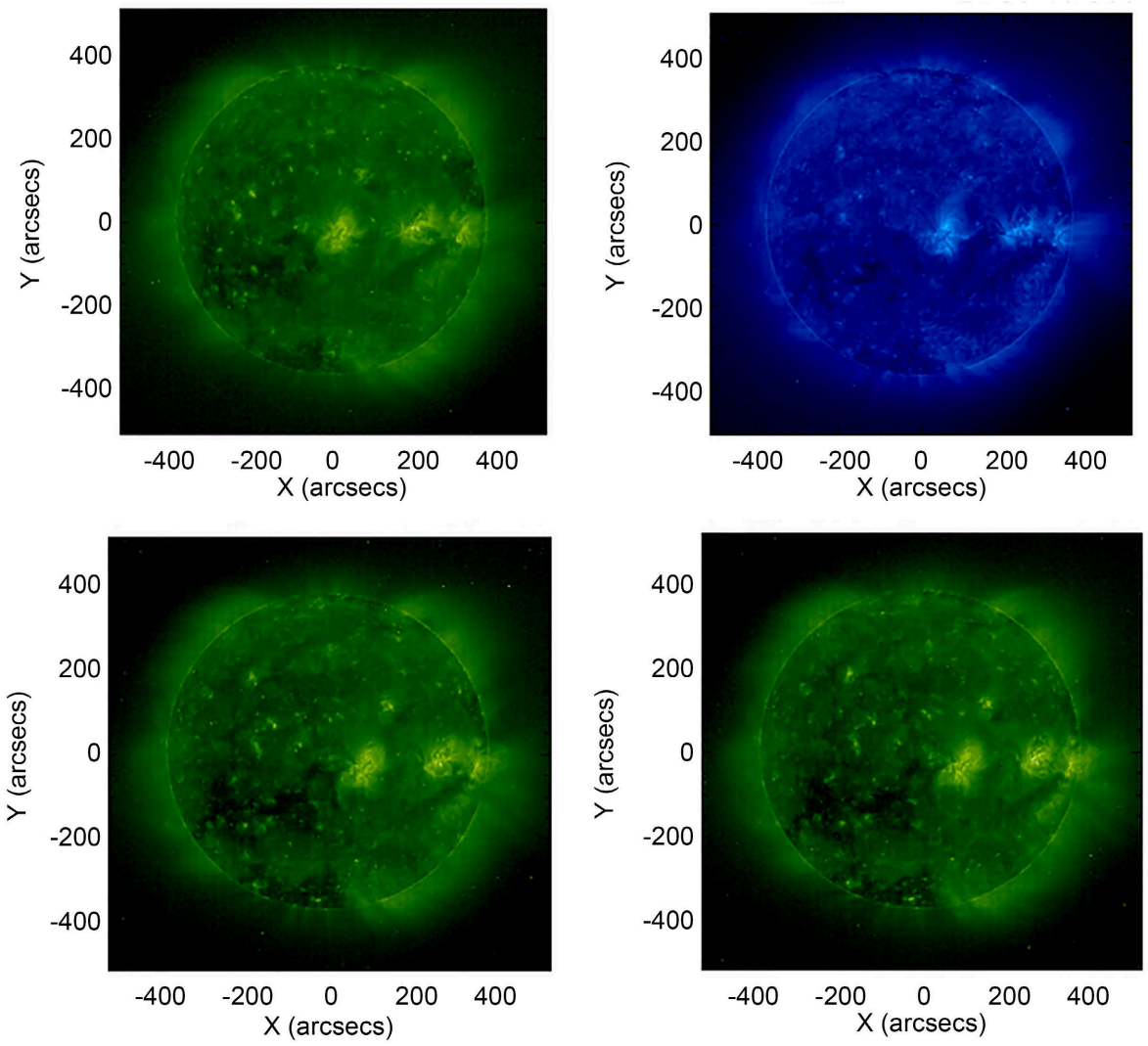

Figure 7. EUV Images from EIT/SOHO in April. 01 (2008). Upper left panel 19.5 nm image at 01:06 UT. Upper right panel 17.1 nm image at 13:00:13 UT. Lower left panel 19.5 nm image at 19:25:05 UT. Lower right panel 19.5 nm image at 23:48:09 UT.

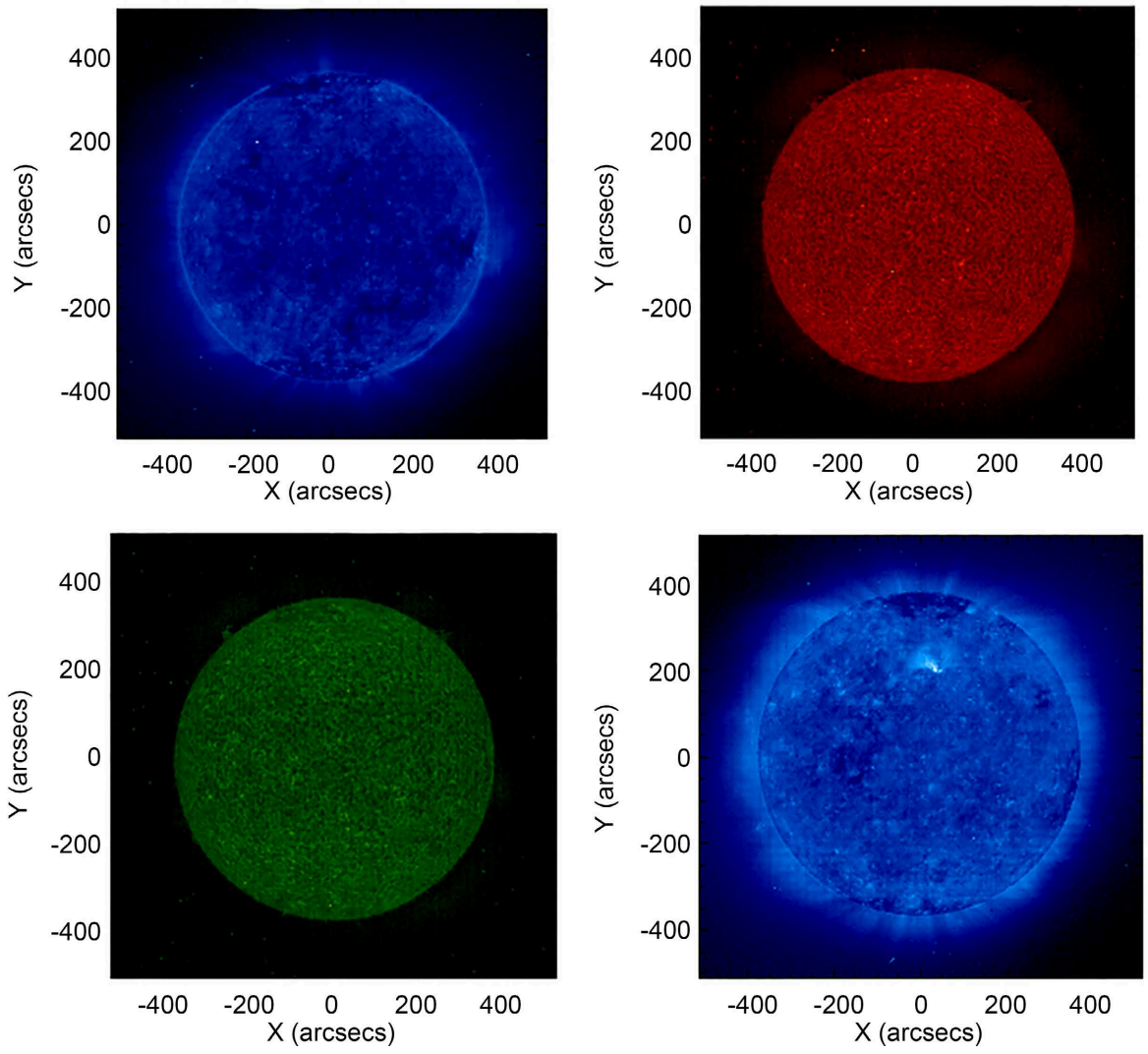

Figure 8. EUV images from EIT/SOHO on Jun 01 (2008). Upper left panel 17.1 nm image at 01:01:13 UT. Upper right panel 30.4 nm image at 07:19:34 UT. Lower panel 19.5 nm image at 23:45:07 UT.

shown in **Figure 9** (Nov. 1, 2008). Finally, **Figure 10** shows in four images (Jan. 1, 2009) the closest, 4 months to solar minimum conditions in the low corona. In summary, **Figures 7-10** show a march in time of the solar corona toward solar minimum, in which few features stand out, besides the fact that in Jan 2009, the presence of CHs of which the most prominent are near the poles.

The minimum between cycles 23 and 24 is particularly interesting. Its temporal extent, it is not seen before during the space-era of sophisticated exploration of the Sun and its environment remote and *in-situ* for some of its solar wind larger manifestations. This solar minimum exhibits unprecedented properties. At solar minimum times, the GOES under-counting effect for weak flares becomes less significant. But it appears to be the case that CMEs continued to occur, although large flares basically ceased in 2008 (only one M-class and 8 C-class flares, see, e.g., records stored by NOAA at its World Wide Web location).

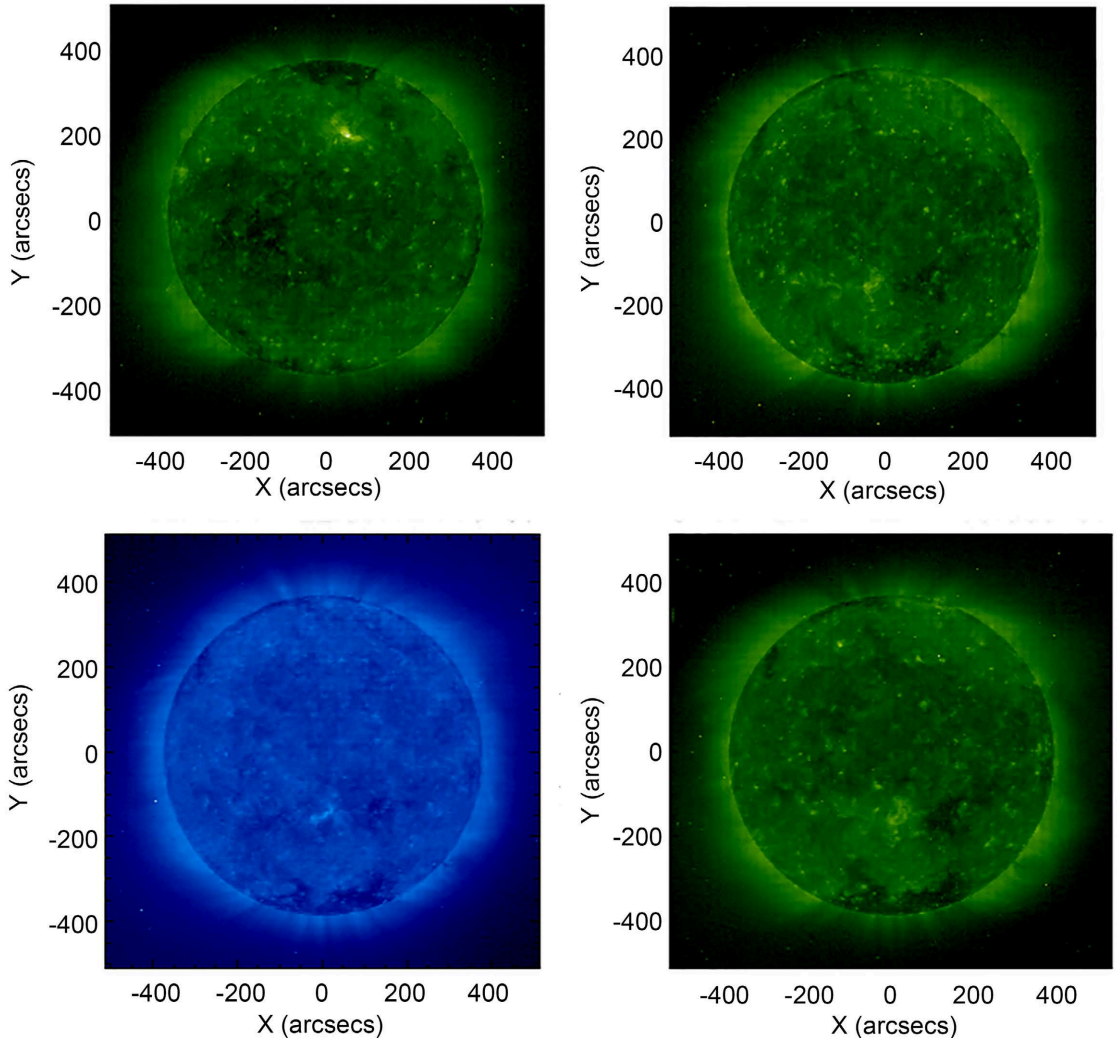

Figure 9. EUV images from EIT/SOHO on Nov 01 (2008). Left upper panel 19.5 nm image at 00:00:11 UT. Upper right panel 19.5 nm image at 12:24:10 UT. Lower left panel 17.1 nm image at 18:00:13 UT. Lower right panel 19.5 nm image at 23:36:09 UT

It is pointed out by Webb *et al.* 1998 [38]; Robbrecht, Patsourakos, Vourlidas, 2009 [39]; Hudson and Li, 2010 [40], that the weaker coronal magnetic field at minimum times is easier to disrupt, in consequence, the CMEs can occur in major frequency. This is an assumption that appears to be corroborated by changes in the frequency of observation of solar transients in the SW at the Earth's Lagrange point L1, see e.g., Lepping *et al.* 2011 [41].

3.2. The 1 AU (*In-Situ*) Manifestations and Its Remote Solar Corona N_e and T_e

Solar Wind (SW) high-speed stream(s) observed at heliospheric ecliptic region at 1 AU, in **Figure 11** show the imprints of solar corona equatorial holes likely always present in the solar minimum period low latitude, although strongly reduced or absent near the actual minima (June 1996 in a previous solar minimum, and April 2009 in the most recent one, see e.g., Steinhilber, 2010 [42]). Indeed, at

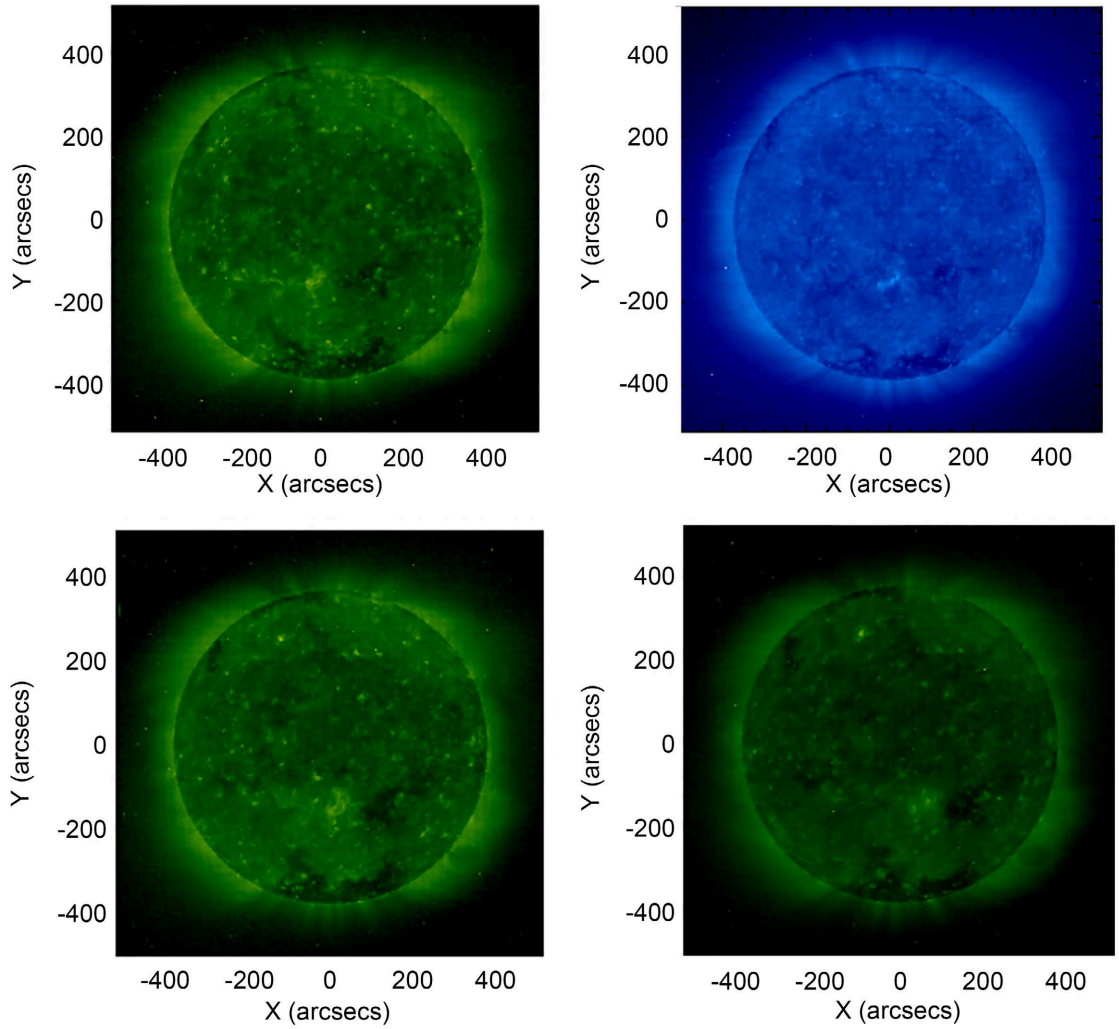

Figure 10. EUV images from EIT/SOHO on Jan 01 (2009). Left upper panel: 19.5 nm image at 00:00:08 UT. Upper right panel: 17.1 nm image at 07:0012 UT. Lower left panel: 195 nm image at 12:48:09 UT. Lower right panel: 19.5 nm image at 23:36:09 UT.

Carrington rotations containing solar minimum co-rotating high-speed solar wind cease or their speeds are highly diminished as the Carrington figures[2] for them to show in **Appendix 2**. In the interval of our study, we noticed that sporadic sunspots seemed to produce more complex, and long-lived active regions.

Figure 11(a) illustrates for April-May 2008 a more complex, both in average and mean faster SW, than the later observed simpler overall SW in **Figure 11(b)** from July-August 2008. It is worth noticing that the circumstantial greater complexity in the SW matches the more complex changes in density N_e of **Figure 1** for the solar minimum and specific to this study **Figure 3** for April-May rather than after June 2008 when there are simpler smooth variations in N_e that reach in about nine more months the lowest values—solar minimum—on or about April 2009. Conditions starting about June 2008 are the ones that match the simpler observed conditions of the SW of **Figure 11(b)**. Be warned that global remote sens-

[2]https://cdaweb.gsfc.nasa.gov/cgi-bin/gif_walk?plot_type=wind_27_day_kp_plots

ing of the quiescent Corona here is compared to a single *in-situ* measurement at the Earth's L1 location in the SW.

When comparing *in-situ* observations with conditions in the quiescent solar corona it is relevant to keep in mind that the location of the disk at the solar minimum region with the bulk of plasma emanating from the quiescent Sun corona possibly concentrates in a narrow region of space beyond several solar radii centered at the Sun equatorial plane. The Sun equatorial and the ecliptic planetary planes intersect solely in the first week of June and December. The observed at the solar minimum in 1996 and 2009 SW speeds at 1 AU in the ecliptic plane are consistent with this understanding of a narrow disk of plasma with this slow SW at the solar equatorial plane. For more definitive connections between SW observations and the quiescent Sun corona it will be useful to have a thorough study beyond the scope of the present one with simultaneous in time observation at other locations of the SW as they are available from STEREO, Messenger, and Luna Observer and possible other missions, Solar Probe recently launch will be of great help in this regard.

Solar irradiance in the interval of time between 2008-2009 appears to indicate that the flux emergence reaches a lower level; while the existing magnetic flux flow evolved causing changes in the large-scale magnetic field that seem to diminish the presence of the equatorial CHs as solar minimum approached, see e.g., Richardson and Cane, 2012 [43]. In conclusion we understand that the frozen

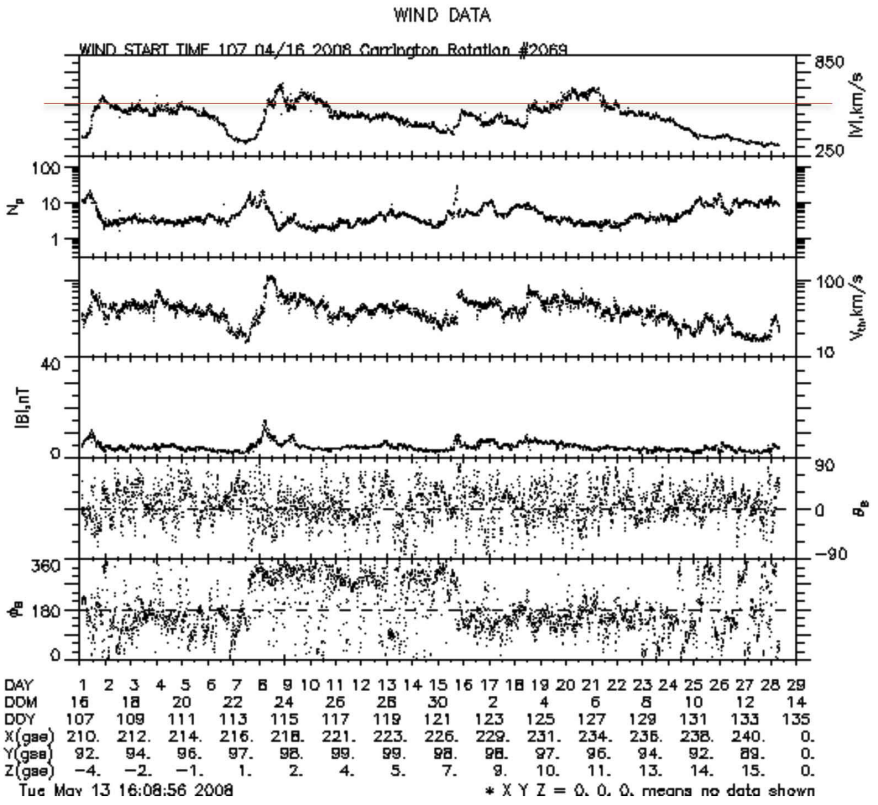

(a)

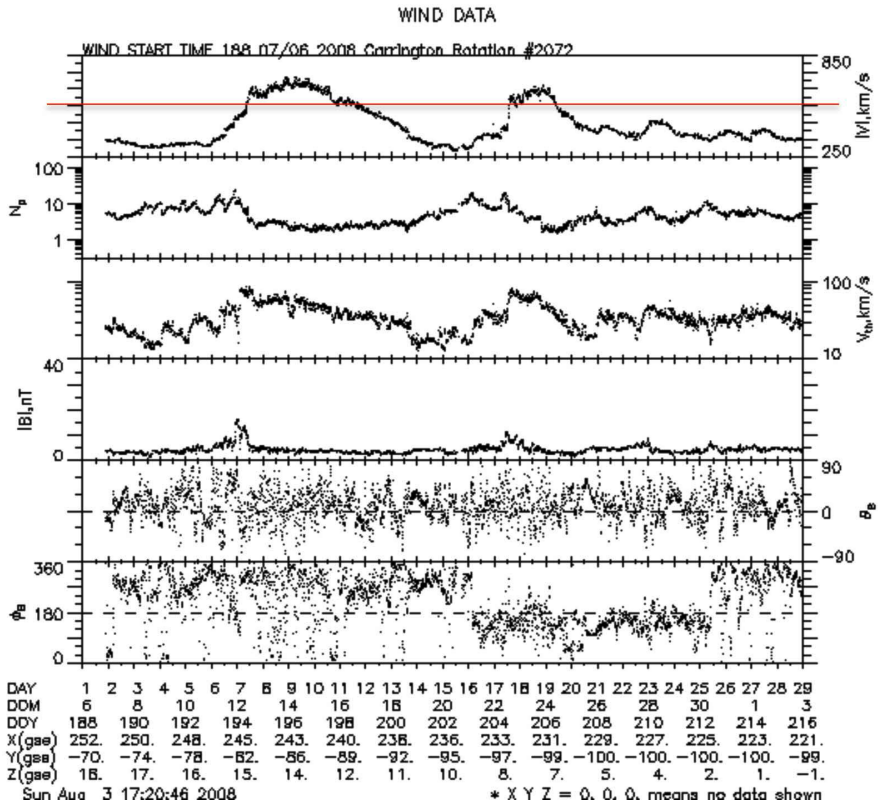

(b)

Figure 11. (a) As a function of time (Carrington rotation number 2069, starting time on May 16, 2008) shown are the solar wind "key" parameters collected at 1 AU by the Wind SC; 1) $|\boldsymbol{V}|$ is the convection velocity of the magnetized solar wind plasma, primarily away from the Sun, 2) N_p is the proton density, 3) V_{th} is the thermal proton velocity, corresponding to a $T_p = V_{th}\sqrt{k/2m_p}$, 4) $|\boldsymbol{B}|$ is the magnitude of the convected in the plasma magnetic field, 5) ϑ_B is the angular direction of $\boldsymbol{B}$ respect to the ecliptic plane, 6) ϕ_B is the angular azimuth direction of $\boldsymbol{B}$ in the ecliptic plane. The bottom-top line counts the number of days included, 2nd bottom line reports the day of the month (DOM), 3rd row gives the day of the year (DOY), 4th row indicates in X-axis along with Sun—Earth line the SC Wind location from the center of the Earth in Earth's radius, completing the location of the SC Wind 5th and 6th lines give in GSE coordinate system the location in the Y along azimuth positive in the direction of the Earth motion around the Sun, and Z positive for North from the ecliptic, completing in this way a right-hand coordinate system[3]. (b) Carrington rotation number 2072, starting time on July 6, 2008[4].

in-situ high-speed streams in 2008 confirm that there was in the Sun corona altitude range of this study a presence of "*unipolar*" magnetic regions at mid to low latitudes related to the CHs (Schrijver *et al.* 2011 [44]; de Toma *et al.* 2010 [45]). These CHs appear to directly relate to the lowest EUV radiation values present in some regions of the low corona, CHs regions that appear to decrease from Jan. 2008 to Jan. 2009 in **Figures 7-10**.

That decrease in CHs area suggests (the source of the fast solar wind) dimini-

[3]https://cdaweb.gsfc.nasa.gov/cgi-bin/gif_walk, Plot type wind 27 days survey, specific date 2008107.
[4]https://cdaweb.gsfc.nasa.gov/cgi-bin/gif_walk, Plot type wind 27 days survey, specific date 2008189.

shing as time passes, see **Appendix 2**. And that decrease expresses in the reduction of the high-speed stream regions in Carrington rotation as shown in **Figure 11** as well as the added intervals in **Figure A2(a)** and **Figure A2(b)**. This interpretation enables our understanding that irradiance collected from 1 AU since the start of 2008 is marginally sensitive to CHs. *i.e.*, the *irradiance is dominated by the one generated from the quiescent* corona with relatively higher radiance values than in CHs regions. This further implies that irradiance is sensitive mainly to the *parallel to the Sun surface field lines in the altitudes of interest.* **Figure 6(b)** shows remote direct measurement at the total Solar Eclipse, August 2008, which as discussed are supportive of the CODET model prediction of the corona T and density (N_e) profiles. These time dependence profiles of N_e show negligible change after June 2008 (**Figure 3**), and temperature (T_e) profiles do not show more significant changes already since April 2008 (**Figure 3**). However, the average energy density (**Figure 4**) related to the variations of the magnetic field showed an increase in April 2008, in agreement with the behavior in the solar atmosphere, some ARs appeared in this period (**Figure 7**). In the same way, the average magnetic and kinetic pressure shows an increase in April 2008 (**Figure 5**).

Notice that in our one-year time interval, the final period June 2008 to January 2009 shows in **Figures 3-5** smaller than before variations in N_e average electron energy density, average magnetic and kinetic electron pressure, and a constant temperature, T_e related to features of the quiet corona which are central to the interpretations in the simple thermodynamics' models presented in Berdichevsky *et al.* 2020 [46] (arXiv preprint paper).

4. Global Manifestation of Low Corona

On the insulation between the quiescent corona and other features with a different temperature shows in Nikolsky *et al.* 1971 [47], near the time of a solar maximum, a clear example describing conditions in the region of the Sun corona, between a quiescent corona with $T > 10^6$ K and a prominence having a much larger mass, and temperature two orders of magnitude smaller (10^{11} e/cm^3 and 10^4 K). Another interesting aspect of the study is the observation of non-thermal contributions to the width of Sun corona non-thermal lines. When split between the line of sight and transverse to that at the base of the corona, the obtained velocity was (10, 25, 25 kms^{-1}). During the eclipse, a great degree of inhomogeneity in the e-density in the "quiescent corona" was estimated, suggesting a possible turbulent activity. Here we speculate that it could also be possible that there was a contribution to the inhomogeneity from some unresolved streamers for this thoroughly described eclipse that corresponded to the active part of the solar cycle, March 7, 1971.

Under the solar minimum conditions of August 1, 2008, total solar eclipse, Habbal *et al.* 2010 [26] present a discussion that is devoted to an interval in altitude in the corona that contains this study's range. Their work distinguished between

two essentially different regions, the one near the poles where with the help of the Fe X and XI a temperature close to 10^6 K is identified. This result appears to agree with the high-speed SW, out of the ecliptic measured Fe frozen charge states in Gloeckler and Geiss, 2007 [48]. For the quiescent corona, the temperature identified in Habbal *et al.* 2010 [26] is consistent with the CODET model illustrated in **Figure 3**.

4.1. The Low Solar Corona Temperature from Thermal Equipartition of Iron Ionization States

Defined from emissions in lines of iron the analysis of the observations of the intensity of the Fe X and XIV charge states during the total eclipse of August 1, 2008, observed in Novosibirsk the detailed analysis in Voulgaris, *et al.* 2010 [25] concludes that the observed radiances of Fe XIV set an upper limit to the quiescent Sun corona temperature of 1.9×10^6 K. The strong radiance of the Fe X line sets a lower boundary to the corona temperature of 1.2×10^6 K. This is a range that contains the value that the CODET model gives to the electron temperature in the region of the study during the year 2008. For other work on the solar minimum in which a more complete description of Fe charge states exists, see e.g., Habbal *et al.* 2010 [26], Daw *et al.* 2010 [27].

We consider the bulk of the irradiance in our study's temperature during the total eclipse of August 1, 2008. Habbal *et al.* 2010 [26] find that the thermal temperature of the quiescent corona has a value constrained between 1.6 and 1.9×10^6 K. During the eclipse of August 1, 2008, Habbal *et al.* 2008 [49] divide the non-polar coronal hole regions into regions where there are streamers and no streamers identified at the base of the corona. The regions classified as non-streamers appear to be harder to observe having a weaker signal in the Fe charge states. Still, in both cases, an estimate for the electron's temperature suggests the observation of mainly Fe XIII and XIV nonthermal emission indicating a temperature like the one observed in the streamers at altitude $\leq 1.3 R_\odot$.

4.2. The Temperature of the Low Solar Corona from the Width of the Iron Non Thermal Lines

The width of optical lines in iron isotopes, non-thermal light emissions in coronograph C1 in SOHO, Mierla *et al.* 2008 [50], present a study between August 1 and October 31, 1996, an interval containing the minimum between solar cycle 22 - 23. The study shows that in the Sun corona between 1.10 and $1.80 R_\odot$ the Fe X 636.6 nm signal appears to be wider in most cases than the Fe XIV 530.3 nm emission. The consequence of this result suggests that non-thermal effects contribute to the increase in the width of this irradiation line Fe X 637.6 nm, which belongs to a charge state of iron that occurs when its temperature is 10^6 K. Fe XIV is a charge state that occurs when the temperature of the medium is 2×10^6 K.

Further, the Fe X and XIV width consistently show a slight gradient in the

height range of our interest, *i.e.*, the temperature predicted appears close to constant in the height range, as shown in Mierla *et al.* 2008 [50] **Figure 8** right panel. This appears consistent with the CODET prediction for the solar minima of the same temperature in the range discussed from 1.16 to $1.23R_{\odot}$.

Finally, if we assume an equal-partition for the Fe charge states, and considering the two states discussed in this work we obtain—from **Figure 1** top two panels in Mierla *et al.* 2008 [50]—a value for the temperature is given by the following relationship:

$$T = \frac{A\times 2\times 10^{6}\ \mathrm{K} + B\times 10^{6}\ \mathrm{K}}{A+B}$$

where A = radiance (Fe XIV − continuum 530.3 nm) = (174 − 163) radiance/s;

and B = radiance (Fe X − continuum 637.6 nm) = (98.5 − 95.6) radiance/s;

and the resulting temperature is then $T = 1.75 \times 10^{6}$ K for the region 1.13 to $1.25R_{\odot}$.

Although this temperature estimate makes strong assumptions that are at best reasonable under specific conditions of overall homogeneity, it is interesting that it is in quantitative agreement with the CODET prediction from **Figure 3** for the model presented in Section 1.

5. Conclusions

The CODET model's validation and interpretation were presented in this work. We conclude with a listing of the physical interpretation of the remote observational findings of the Sections 3 and 4, as well as at 1 AU *in-situ* manifestations, which in the 2nd part of this work. Also, we include some considerations of our model from Berdichevsky *et al.* 2020 [46], Section 2 (arXiv preprint paper).

The quiescent solar corona in the region of interest appears to be constituted by an *idealized* ensemble of magnetic tubes contained in regions, which are consistent with the assumption of having at their micro-scale level a cylindrical shape, being in an orientation parallel to the Sun's photosphere. Here, we assume them to be regions homogeneous in the limit of the observational resolution capability, *i.e.*, with a cross-section of about πl^{2} and length $(4l)$, with $l \approx 25$ km , from a rough. Previously, estimations at the Sun's corona, TR and chromosphere were obtained in Berdichevsky and Schefers, 2015 [51]. In Berdichevsky *et al.* 2020 [46]—Section 1 (arXiv preprint paper), we will use a value $l = 20$ km .

To extrapolate on the ratio of SW flowing in the streamers away and without return to the solar corona at altitude $1.23R_{\odot}$, the SW contains just a fraction of no more than 1/16 of all masses in the corona region of interest, $1.1 \le r/R_{\odot} \le 1.31$, which is consistent with that region at solar minimum as being the source of the SW (**Figure 11**) from the equatorial solar streamers (**Figure 6**) which exist in the heliosphere plasma-belt enclosing the Parker current sheet. This result allows us to assume that the quiescent solar corona considered contains mainly "matter trapped in closed magnetic field tubes". This is again consistent with the

suggested interpretation of the properties of the matter and magnetic field expressed in the point before (1) (see **Appendix 3**).

In the study of very small presence of filament/prominence eruption, there is no recording of any observation in the Sun-Earth line of sight of any such flux-rope structures from Dec. 2007 to Dec. 2008, the time of the study (Sections 3 and 4). A subgroup of all ejecta is discussed in Lepping *et al.* 2011 [41], and their presence, quite common for all of 2009, which did not seem to affect in any substantial way the prediction made for the nature of the electron's density and temperature for more than 2 years of quiescent Sun corona at the solar minimum of 2009. A more extended interval of identification of solar ejecta of the magnetic field dominated kind containing this solar minimum was present in Wu and Lepping, 2015 [52], see also in **Appendix 4**.

For most of the quiescent intervals there is a presence of some Sun's Coronal Hole (CH) region(s) with a substantial impact at 1 AU, see Section 3 on the generation of a fast speed solar wind, which it is possible to document from *in-situ* observation of the SW at L1. It seems we do not need to address the fundamentally different nature of their thermodynamic properties in this study because the source region is likely of lesser relevance to the global irradiance from $1.1 \le r/R_{\odot} \le 1.31$ (Notice how no signatures of a quantitative influence appear in the CODET model predictions for N_e and T_e across a few Carrington rotations when SW observations show the transition from intervals with high-speed SW to those with slower speed SW while reaching the solar minimum in April 2009, thereby implying an absence of high-speed SW is also an absence of equatorial CHs precisely near the solar minimum in June 2009).

The CODET model electron density and temperature estimations are shown in Section 2 show reasonable agreement with two different direct inferences on T_e presented in Section 4.

It is concluded from all the considered observables discussed in Section 3 that there exists an active mechanism responsible for the insulation of the quiescent low Sun's corona, and different structures at the same altitude with different thermal and magnetic properties, *i.e.*, 1) equatorial Coronal Hole(s); 2) filament/prominence(s); 3) small ARs and/or ARs remnants.

The CODET model is shown to be quantitatively accurate in reproducing independent observations obtained by remote sensing during total solar eclipses and the other available remote and *in-situ* observations of the Solar Corona and the Solar Wind.

The fact that thermal insulation occurs in the superior regions of the Sun is dramatically proven during the solar minimum when for extended quiet intervals during the sun activity there is a well-known massive temperature difference between the photosphere and low corona with dramatic variation in value in the Transition Region (TR), just passing the chromosphere (see e.g., Vernazza, Anrett, and Loeser, 1981 [53]). The model (Berdichevsky *et al.* 2020 [46]—Section 2 arXiv preprint paper) presents interpretations of the constitutive nature of the magnetized

matter that populates the corona between 1.1 and 1.3$R_{\odot}$ and is consistent with indicated observations in Section 3.

Acknowledgements

D.B.B. thanks his father Carlos David for his loving support of a whole life. Furthermore, D.B.B.'s work is offered in the memory of his loved wife, the late Maria-Cristina Beatriz. J.M.R.G thanks Skoltech for the partial support of this work.

Conflicts of Interest

The authors declare no conflicts of interest regarding the publication of this paper.

References

[1] Judge, P.G. (1998) Spectral Lines for Polarization Measurements of the Coronal Magnetic Field. I. Theoretical Intensities. *The Astrophysical Journal*, **500**, 1009-1022. https://doi.org/10.1086/305775

[2] Gómez, J.M.R., Vieira, L., dal Lago, A. and Palacios, J. (2018) Coronal Electron Density, Temperature and Solar Spectral Irradiance during Solar Cycles 23 and 24. *The Astrophysical Journal*, **852**, Article No. 137, 11p. https://doi.org/10.3847/1538-4357/aa9f1c

[3] Morgan, H. and Taroyan, Y. (2017) Global Conditions in the Solar Corona from 2010 to 2017. *Science Advances*, **3**, Article ID: e1602056. https://doi.org/10.1126/sciadv.1602056

[4] Gómez, J.M.R. (2017) Evolution of the Electron Density, Temperature Distribution in the Solar Corona during Solar Cycles 23 and 24, Ph.D. Thesis, Instituto Nacional de Pesquisas Espaciais (INPE). http://urlib.net/8JMKD3MGP3W34P/3NCJQLB

[5] Aschwanden, M. (2019) New Millennium Solar Physics. Astrophysics and Space Science Library, Vol. 458, Springer, Cham. https://doi.org/10.1007/978-3-030-13956-8

[6] Scherrer, P.H., Bogart, R.S., Bush, R.I., Hoeksema, J.T., Kosovichev, A.G., Schou, J., Rosenberg, W., Springer, L., Tarbell, T.D., Title, A., Wolfson, C.J., Zayer, I. and The MDI/SOHO Engineering Team (1995) The Solar Oscillations Investigation-Michelson Doppler Imager. *Solar Physics*, **162**, 129-188. https://doi.org/10.1007/BF00733429

[7] Scherrer, PH, Schou, J., Bush, R.I., Kosovichev, A.G., Bogart, R.S., Hoeksema, J.T., Liu, Y., Duvall, , T.L.J., Zhao, J., Title, A.M., Schrijver, C.J., Tarbell, T.D. and Tomczyk, S. (2012) The Helioseismic and Magnetic Imager (HMI) Investigation for the Solar Dynamics Observatory (SDO). *Solar Physics*, **275**, 207-227. https://doi.org/10.1007/s11207-011-9834-2

[8] Schrijver, C.J. (2001) Simulations of the Photospheric Magnetic Activity and Outer Atmospheric Radiative Losses of Cool Stars Based on Characteristics of the Solar Magnetic Field. *The Astrophysical Journal*, **547**, Article No. 475. https://doi.org/10.1086/318333

[9] Schrijver, C.J. and De Rosa, M.L. (2003) Photospheric and Heliospheric Magnetic Fields. *Solar Physics*, **212**, 165-200. https://doi.org/10.1023/A:1022908504100

[10] Del Zanna, G., Dere, K.P., Young, P.R., Landi, E. and Mason, H.E. (2015) CHIANTI—An Atomic Database for Emission Lines. Version 8. *Astronomy & Astrophysics*, **582**, Article No. A56. https://doi.org/10.1051/0004-6361/201526827

[11] Charbonneau, P. (1995) Genetic Algorithms in Astronomy and Astrophysics. *The Astrophysical Journal Supplement*, **101**, 309-334. https://doi.org/10.1086/192242

[12] Mathews, J. and Walker, R.L. (1970) Mathematical Methods of Physics. 2nd Edition, Addison-Wesley World Student Series, Benjamin, Menlo Park.

[13] Robbrecht, E., Wang, Y.-M., Sheeley, N.R. and Rich, N.B. (2010) On the "Extended" Solar Cycle in Coronal Emission. *The Astrophysical Journal*, **716**, 693-700. https://doi.org/10.1088/0004-637X/716/1/693

[14] Yokoyama, T. and Shibata, K. (2001) Magnetohydrodynamic Simulation of Solar Flare with Chromospheric Evaporation Effect Based on the Magnetic Reconnection model. *The Astrophysical Journal*, **569**, 1160-1174. https://doi.org/10.1086/319440

[15] Golub, L. (1983) Empirical Scaling Laws for Coronal Heating. *Solar and Stellar Magnetic Fields*, *Origins and Coronal Effects*: *Proceedings of the Symposium*, Zürich, 2-6 August 1982, 345-361.

[16] Emslie, A.G. (1985) The Structure of High-Temperature Solar Flare Plasma in Non-Thermal Models. *Solar Physics*, **98**, 281-291. https://doi.org/10.1007/BF00152461

[17] Altschuler, M.D. and Newkirk, G. (1969) Magnetic Fields and the Structure of the Solar Corona. I: Methods of Calculating Coronal Fields. *Solar Physics*, **9**, 131-149. https://doi.org/10.1007/BF00145734

[18] Osherovich, V.A., Gliner, E.B. and Tzur, I. (1985) Theoretical Model of the Solar Corona during Sunspot Minimum, II-Dynamic Approximation, Part 1, *The Astrophysical Journal*, **288**, 396-400. https://doi.org/10.1086/162803

[19] Zirin, H. (1966) The Solar Atmosphere. Translated from English into Russian, Mir, Moskva, 584 p.

[20] Dyson, F.W., Eddington, A.S. and Davidson, C. (1920) A Determination of the Deflection of Light by the Sun's Gravitational Field, from Observations Made at the Total Eclipse of May 29, 1919. *Philosophical Transactions of the Royal Society A*: *Mathematical*, *Physical and Engineering Sciences*, **220**, 291-333. https://doi.org/10.1098/rsta.1920.0009

[21] Delaboudinière, J.-P., Artzner, G.E., Brunaud, J., Gabriel, A.H., Hochedez, J.F. Millier, F., Song, X.Y., Au, B., Dere, K.P., Howard, R.A., Kreplin, R., Michels, D.J., Moses, J.D., Defise, J.M., Jamar, C., Rochus, P., Chauvineau, J.P., Marioge, J.P., Catura, R.C. and Lemen, J.R. (1995) EIT: Extreme-Ultraviolet Imaging Telescope for the SOHO Mission. *Solar Physics*, **162**, 291-312. https://doi.org/10.1007/BF00733432

[22] Ogilvie, K.W., Chornay, D.J., Fitzenreiter, R.J., Hunsaker, E., Keller, J., Lobell, J., Miller, G., Scudder, J.D., Sittler, E.C.J., Torbert, R.B., Bodet, D., Needell, U., Lazarus, A.J., Steinberg, J.T., Tapan, J.H., Mavretic, A. and Gergin, E. (1995) SWE, a Comprehensive Plasma Instrument for the Wind Spacecraft, Spa. *Space Science Reviews*, **71**, 55-77. https://doi.org/10.1007/BF00751326

[23] Lepping, R.P., Acuña, M.H., Burlaga, L.F., Farrell, W.M., Slavin, L.A., Schatten, K.H., Mariani, F., Ness, N.F., Neubauer, F.M., Whang, Y.C., Byrnes, J.B., Kennon, R.S., Panetta, P.V., Scheifele, J. and Worley, E.M. (1995) The Wind Magnetic Field Investigation, Spa. *Space Science Reviews*, **71**, 207-229. https://doi.org/10.1007/BF00751330

[24] Michels, D.J. and the EIT and LASCO Teams (1998) Organization of the Corona at Solar Minimum. *Proceedings of the* 3*rd SOLTIP Symposium*, Beijing, 14-18 October 1996.

[25] Voulgaris, A., Athanasiadis, T., Seiradakis, J.H. and Pasachoff, J.M. (2010) A Comparison of the Red and Green Coronal Line Intensities at the 29 March 2006 and the 1 August 2008 Total Solar Eclipses: Considerations of the Temperature of the Solar Corona. *Solar Physics*, **264**, 45-55. https://doi.org/10.1007/s11207-010-9575-7

[26] Habbal, S.R., Druckmüller, M., Morgan, H., Daw, A., Johnson, J., Ding, A., Arndt, M.,

Esser, R., Rusin, V. and Scholl, I. (2010) Mapping the distribution of Electron Temperature and Fe Charge States in the Corona with Total Eclipse Observations. *The Astrophysical Journal*, **708**, 1650-1662. https://doi.org/10.1088/0004-637X/708/2/1650

[27] Daw, A., Habbal, S.R., Morgan, H., Druckmüller, M., Ding, A., Johnson, J. and Rusin, V. (2009) Eclipse Observations of the Fe XI 789.2 nm Line. *Bulletin of the American Astronomical Society*, **41**, 323.

[28] Sheeley, N.R.J., Wang, Y.-M., Hawley, S.H., Brueckner, G.E., Dere, K.P., Howard, R.A., Koomen, M.A., Korendyke, C.M., Michels, D.M., Paswaters, S.E., Socker, D.G., Cyr, O.C.S., Wang, D., Lamy, P.L., Llebaria, A., Schwenn, R., Simnett, G.M., Plunkett, S. and Biesecker, D.A. (1997) Measurements of Flow Speeds in the Corona between 2 and 30 *R*. *The Astrophysical Journal*, **484**, 472-478. https://doi.org/10.1086/304338

[29] Dere, K.P., Howard, R.A. and Brueckner, G.E. (2000) Coronal Mass Ejections and the Solar Wind: New Results from LASCO. *Advances in Space Research*, **25**, 1837-1842. https://doi.org/10.1016/S0273-1177(99)00594-3

[30] Vasquez, B.J., Farrugia, C.J., Simmunac, K.D.C., Galvin, A.B. and Berdichevsky, D.B. (2017) Concerning the Helium-to-Hydrogen Number Density Ratio in Very Slow Ejecta and Winds near Solar Minimum. *Journal of Geophysical Research*: *Space Physics*, **122**, 1487-1512. https://doi.org/10.1002/2016JA023636

[31] Viall, N.W. and Vourlidas, A. (2015) Periodic Density Structures and the Origin of the Slow Solar Wind. *The Astrophysical Journal*, **807**, Article No. 176. https://doi.org/10.1088/0004-637X/807/2/176

[32] Sanchez-Diaz, E., Rouillard, A.P., Lavraud, B., Segura, K., Tao, C., Pinto, R., Sheeley, N.R.J. and Plotnikov, I. (2016) The Very Slow Solar Wind: Properties, Origin and Variability. *Journal of Geophysical Research*: *Space Physics*, **121**, 2830-2841. https://doi.org/10.1002/2016JA022433

[33] Priest, E. (2014) Magnetohydrodynamics of the Sun. Cambridge University Press, Cambridge, UK.

[34] Schwenn, R. and Marsch, E. (1990) Physics of the Inner Heliosphere. Vol. I, Springer Verlag, Berlin. https://doi.org/10.1007/978-3-642-75361-9

[35] De Pontieu, B., McIntosh, S.W., Hansteen, V.H. and Schrijver, C.J. (2009) Observing the Roots of Solar Coronal Heating-In the Chromospheres. *The Astrophysical Journal*, **701**, L1. https://doi.org/10.1088/0004-637X/701/1/L1

[36] De Pontieu, B, McIntosh, S.W., Carlsson, M., Hansteen, V.H., Tarbell, T.D., Boerner, P., Martinez-Zycora, J., Schreiver, C.J. and Title, A.M. (2011) The Origins of Hot Plasma in the Solar Corona. *Science*, **331**, 55-58. https://doi.org/10.1126/science.1197738

[37] Gomez, D.O., Bejarano, C. and Mininni, P.D. (2014) Kelvin-Helmholtz versus Hall Magneto Shear Instability in Astrophysical Flows. *Physical Review E*, **89**, Article ID: 053105. https://doi.org/10.1103/PhysRevE.89.053105

[38] Webb, D.F., Cliver, E.W., Gopalswamy, N., Hudson, H.S. and Cyr, O.C.S. (1998) The Solar Origin of the January 1997 Coronal Mass Ejection, Magnetic Cloud and Geomagnetic Storm. *Geophysical Research Letters*, **25**, 2469-2472. https://doi.org/10.1029/98GL00493

[39] Robbrecht, E., Patsourakos, S. and Vourlidas, A. (2009) No Trace Left Behind: Stereo Observations of a CME without Low Coronal Signatures. *Astrophysical Journal*, **701**, Article No. 283. https://doi.org/10.1088/0004-637X/701/1/283

[40] Hudson, H.S. and Li, Y. (2010) Flare and CME Properties and Rates at Sunspot Minimum. In: Cranmer, S.R., Hoeksema, J.T. and Kohl, J.L., Eds., *SOHO*-23: *Understanding a Peculiar Solar Minimum*, ASP Conference Series, Vol. 428, Astronomical Society of the Pacific, San Francisco, 153-160.

[41] Lepping, R.P., Wu, C.-C., Berdichevsky, D.B. and Szabo, A. (2011) Magnetic Clouds

at/near 2007-2009 Solar Minimum: Frequency of Occurrence and Some Unusual Properties. *Solar Physics*, **274**, 345-360. https://doi.org/10.1007/s11207-010-9646-9

[42] Steinhilfber, F. (2010) Total Solar Irradiance since 1996: Is There a Long-Term Variation Unrelated to Solar Surface Magnetic Phenomena. *Astronomy & Astrophysics*, **523**, Article No. A39. https://doi.org/10.1051/0004-6361/200811446

[43] Richardson, I.G. and Cane, H. (2012) Near-Earth Solar Wind Flows and Related Geomagnetic Activity during More than Four Solar Cycles. *Journal of Space Weather and Space Climate*, **2**, Article No. A02. https://doi.org/10.1051/swsc/2012003

[44] Schrijver, C.J., Livingston, W.C., Woods, T.N. and Mewaldt, R.A. (2011) The Minimal Solar Activity in 2008-2009 and Its Implications for Long-Term Climate Modeling. *Geophysical Research Letters*, **38**, Article ID: L06701. https://doi.org/10.1029/2011GL046658

[45] De Toma, G., Gibson, S.E., Emery, B.A. and Arge, C.N. (2010) The Minimum between Cycle 23 and 24: Is Sunspot Number the Whole Story? In: Cranmer, S.R., Hoeksema, J.T. and Kohl, J.L., Eds., *SOHO*-23: *Understanding a Peculiar Solar Minimum*, ASP Conference Series, Vol. 428, Astronomical Society of the Pacific, San Francisco, 217-222.

[46] Berdichevsky, D., Gómez, J.M.R., Viera, L. and Dal Lago, A. (2020) Thermodynamics Interpretation of Electron Density and Temperature Description in the Solar Corona. arXiv:2005.07929. http://arxiv.org/abs/2005.07929

[47] Nikolsky, G.M., Gulyaev, R.A. and Nikolskaya, K.I. (1971) Spectrophotometry of the Corona and a Quiescent Prominence Based on Observations of the Total Solar Eclipse of 7 March, 1970 in Mexico. *Solar Physics*, **221**, 332-350. https://doi.org/10.1007/BF00154285

[48] Glockler, G. and Geiss, J. (2007) The Composition of the Solar Wind in Polar Coronal Holes. *Space Science Reviews*, **130**, 139-152. https://doi.org/10.1007/s11214-007-9189-z

[49] Habbal, S.R., Scholl, I.F. and McIntosh, S.W. (2008) Impact of Active Regions on Coronal Hole Outflows. *The Astrophysical Journal Letters*, **683**, Article No. L75. https://doi.org/10.1086/591315

[50] Mierla, M., Schwenn, R., Teriaca, L., Stenborg, G. and Podlipnik, B. (2008) Analysis of the Fe X and Fe XIV Line Width in the Solar Corona Using LASCO-C1 Spectral Data. *Astronomy & Astrophysics*, **480**, 509-514. https://doi.org/10.1051/0004-6361:20078329

[51] Berdichevsky, D.B. and Schefers, K. (2015) On the Thermodynamics and Other Constitutive Properties of a Class of Strongly Magnetized Matter Observed in Astrophysics. *The Astrophysical Journal*, **805**, Article No. 70. https://doi.org/10.1088/0004-637X/805/1/70

[52] Wu, C.-C. and Lepping, R.P. (2015) Comparison of Characteristics of Magnetic Clouds and Magnetic Cloud-Like Structures during 1995-2012. *Solar Physics*, **290**, 1243-1269. https://doi.org/10.1007/s11207-015-0656-5

[53] Vernazza, J.E., Avrett, E.H. and Loeser, R. (1981) Structure of the Solar Chromosphere. III. Models of the EUV Brightness Components of the Quiet Sun. *Astrophysical Journal*, **45**, 635-725. https://doi.org/10.1086/190731

[54] Berdichevsky, D., Geiss, J., Gloeckler, G. and Mall, U. (1997) Excess Heating of $^4He^{2+}$ and O^{6+} relative to H^+ Downstream of Interplanetary Shocks. *Journal of Geophysical Research*: *Space Physics*, **102**, 2623-2635. https://doi.org/10.1029/96JA02541

Appendix 1

With Figure A1, we assume for simplification a simply spherical geometric shape of the Sun. Here we look at it just from the perspective of its projection onto the plane of the sky. Further we use the spherical coordinate θ to distinguish the two principal solar corona regions, the ones of the polar CH at the solar minimum from the region we consider to be mainly of the quiescent corona. θ shown in Figure A1, is the apparent limit between these two regions. This occurs approximately at $\theta \approx 30^{\circ}$. This is the situation corresponding to the coronal hole at the time interval of minimal activity in the solar cycle, *i.e.*, encompassing the solar minimum. The corresponding area of irradiance observed at the time, shown as a projection in the plane of the sky in Figure A1. It can be obtained from the integral:

$$A_{\text{coronal hole}} = \frac{1}{2} r^2 \int_0^{2\pi} \mathrm{d}\phi \int_0^{\pi/6} \mathrm{d}\pi$$

with two coronal hole regions symmetric to each other, the area from which the irradiance of the Sun remotely observed is $2A_{\text{coronal hole}}$ while the semi-sphere area is $A_{\text{semi-sphere}} = 2\pi R^2$. Then, we consider:

$$A_{\text{semi-sphere}} - 2A_{\text{coronal hole}}$$

Hence, the percent of irradiance resulting from the quiescent Sun corona we consider is:

$$\frac{100\left[A_{\text{semi-sphere}} - 2A_{\text{coronal hole}}\right]}{A_{\text{semi-sphere}}} = 86.6\%$$

and when we consider that the irradiance from the coronal hole region appears suppressed compared to the one, we use, essentially, we can neglect that part as a contribution in the modeling of the corona irradiance as a function of the high in the low corona.

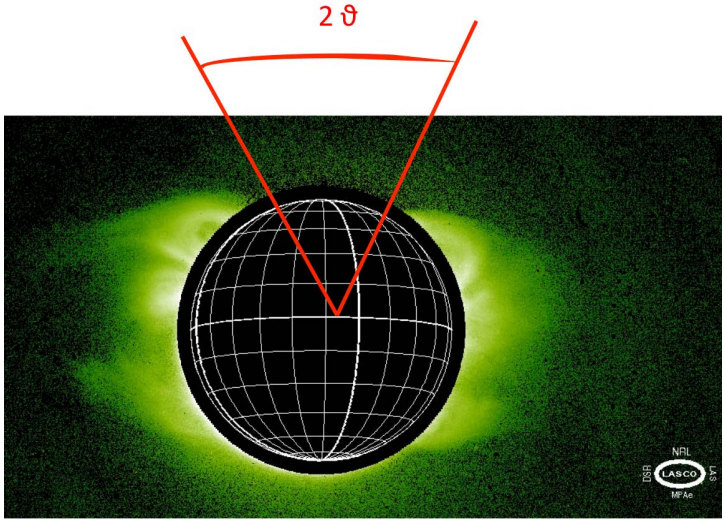

Figure A1. The quiescent Solar Corona in Fe XIV, the region source of the slow solar wind. Borrowed from the WWW site of the LASCO/SOHO mission.

Appendix 2

Figure 11 shows SW parameters for intervals of 27 days each corresponding to April-May and July-August respectively. From top to bottom panels display $|\boldsymbol{V}_{\mathbf{SW}}|$ the magnitude of the convection velocity of steady state magnetized matter, its key attributes described in Parker, 1958, 2nd from the top is the proton density. 3rd the protons kinetic energy distribution in the SW frame of reference (V_{th} in the common language of Helio-physics). The 4th, 5th and 6th panel from the top respectively give the magnitude and angular orientation of the frozen matter magnetic field in the SW.

In the 1st panel conventional conditions associated with the convection of the heliospheric plasma away from the Sun are marked, distinguishing slow from intermediate (red line) and intermediate from fast (black) SW. The solar wind with speed above the black line is well tested to originate at a solar coronal hole, in this case an equatorial solar coronal hole. The solar wind at above 700 km·s^{-1} is understood to be unimpeded solar wind from a CH. Between 500 km·s^{-1} and 300 km·s^{-1} is a region resulting from a variety of coronal regions, they often also include transients (interplanetary manifestations of coronal mass ejections ICME). The nature of the solar wind from the intermediate region is not easy to connect to a specific solar region and tends to show large fluctuations in the orientation of the magnetic field, panels 6th, 7th, and 8th. Before a high-speed stream with origin in a CH region, there is the known Co-rotating Interaction Region (CIR) where the intermediate or slow solar wind is compressed showing an enhancement in density (2nd panel) and magnetic field intensity (4th panel). In the case of it being overtaken by an interplanetary shock the proton thermal velocity V_{th} will often show a substantial increase. The alfvenic behavior of the fast speed solar wind in the 5th and 6th panels shows strong, nearly periodic oscillation of the magnetic field while the intensity stays without variation. The azimuth angle shows the polarity of the CH region and often with extreme accuracy (away or inward from the location of the Sun). When comparing the period intervals of Figure 11 it is striking to notice in both cases the equatorial presence of CHs in the corona and in Figure 11(b) the near absence of very slow SW with velocities of 300 km·s^{-1} or less. A simpler SW organization of the in the ecliptic observed SW is seen in Figure 11(b) for the time interval of July-August. Figure 11(b) shows almost the manifestations of the SW from "closed field regions", a denomination that applies well to the quiescent corona central to this study.

Figure A2 shows the same organization as in Figure 11 ($|\boldsymbol{V}_{\mathbf{SW}}|$ in the 1st panel, N_p in the 2nd, V_{th}, in the 3rd, and the magnetic field intensity and orientation in the 4th, 5th, and 6th panels) appear to indicate a SW that although responsive to the effect of equatorial CH originated SW is at most tangentially impacted while a very slow solar wind appears to be present in the case of Figure A2(a) and the high speed SW almost totally absent during the time nearest to the solar minimum, which was around April 2009.

In all time intervals illustrated, both in Figure 11 as well as Figure A2, the

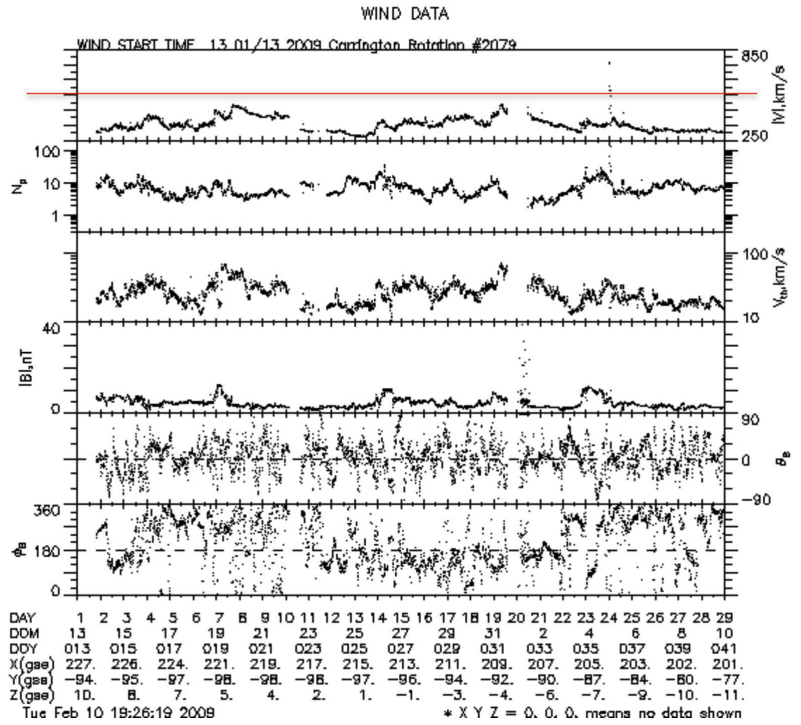

(a)

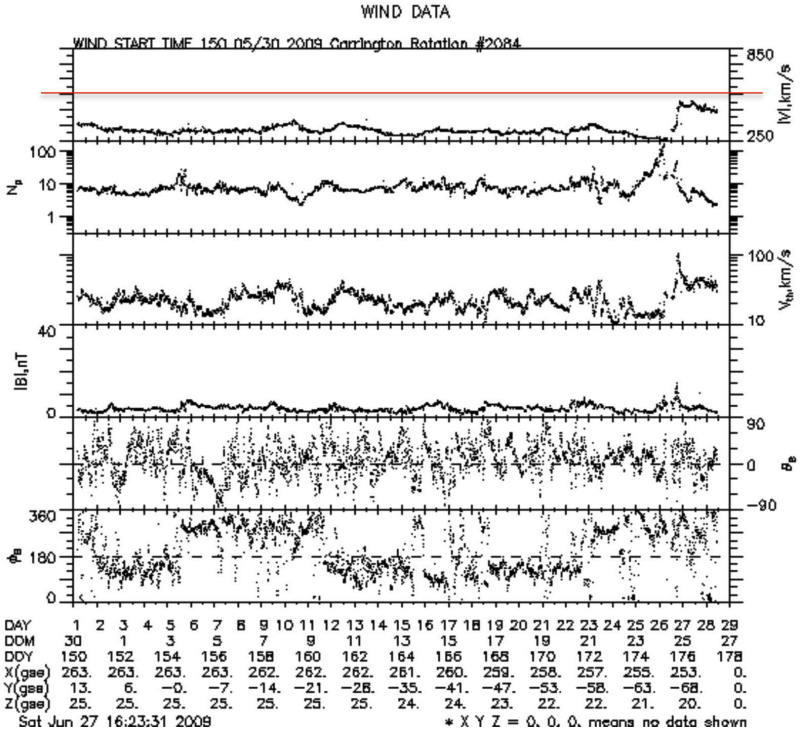

(b)

Figure A2. (a) Similar as **Figure 11** but for Carrington rotation 2079, starting Jan. 13, 2009[5]. (b) Carrington rotation very close to the solar minimum May 30, 2009, Carrington rot. Number 2084[6].

[5]https://cdaweb.gsfc.nasa.gov/cgi-bin/gif_walk, Plot type wind 27 days survey, specific date 200913.

[6]https://cdaweb.gsfc.nasa.gov/cgi-bin/gif_walk, Plot type wind 27 days survey, specific date 2009150.

magnetic field is substantially below long-standing average, and that is true too for the number of particles per cm^3 indicating after Parker that we are dealing with a lesser solar output of energy into the corona, *i.e.*, matter and magnetic field contributing to an unusual cool corona ($<2 \times 10^6$ K).

Appendix 3

Using similar assumptions as in **Appendix 1** for the simple estimates on the geometry considered for the presence of other that quiescent solar corona region that influence the irradiance of the solar corona we are able to estimate both: 1) the e-number of 3×10^7 e/cm^3 at $1.23R_\odot$ as derived via the CODET model for solar minimum consistent with the inverse tomographic determination of e-irradiance in an homogeneous K-corona in years 2008-2010 of minima solar activity; and 2) long time average(s) of particle number from *in-situ* proton measurements [33] (Priest, 2014), which is well approximated by $<p_{1AU}> \sim 10/cm^3$, in which it is relevant to consider that other ions are present with more stripped e than just H^+, see e.g., [54] Berdichevsky *et al.* 1997.

Then it is straightforward to obtain the estimate of the e-number that contribute to the solar K-corona irradiance at $r = 1.23R_e$. This is given by considering the whole region which then becomes part of the equatorial streamers as is shown in **Figure 8**. This number is given as:

$$-\text{Number}(r) \sim 0.9\left(4\pi r^2\right)\text{cm } N_e$$

where 1 cm applies because the evaluation is given for number of particles per cm^3 both in the remote and *in-situ* estimates. Because we are counting over all particles streamed in the SW, using the average here is a good approximation particularly for the case of an interval during solar minimum.

The same estimate at the Lagrange point L1, for the measurement by Wind during a long-time averaging extends the value to all the likely regions of 30˚ width of a slow solar wind heliospheric plasma sheet containing the heliosphere current sheet is reasonable. Hence, the number over this "disc" of particles with the assumption of having an homogeneous outflow equivalent to 2/3 of the whole region, also a strong although reasonable approximation to make, indicates that the total streamers outflow, *i.e.*, the solar wind in regions where *in-situ* observations exist (>0.28 AU) is given by the expression:

$$e-\text{Number}\left(r_{1\,\text{AU}} = 1\,\text{AU}\right) = (2\pi)(20/180)\left(r_{1\,\text{AU}}^2\right)\text{cm } N_{SW}$$

Then, we obtain:

$$e-\text{Number}(r)\Big/e-\text{Number}\left(r_{1\,\text{AU}} = 1\,\text{AU}\right) = 172e$$

which is about 16 times larger than the observed ~$11.2e$ in the SW with origin at the streamers, which was assumed in simplified estimates of total particles at both regions. In addition, we must consider that the inverse evaluation of the e-density from the radiance in the K-corona introduces an uncertainty that can be reasonably assumed to be of about 30%. The uncertainties in the *in-situ* measurement of

SW particles are much smaller, in the range of 1.5 to 3 p per cm^3. In both cases, we deal with larger uncertainties about the simplified assumptions regarding the geometry both in the corona and at 1 AU.

Appendix 4

For estimating the transient presence, we proceed to consider at solar minimum MC, *i.e.*, Magnetic flux-ropes, and those structures lacking—on average—the smooth rotation of the magnetic field and classified by Lepping and co-workers as MC-Like (CL). We consider that these events will be weak, and independent of their latitude of origin, that the dominant polar coronal hole presence will direct them to be located and mostly aligned with solar equator, while having on average an extension of in longitude of 45˚, *i.e.*, 0.28 AU, with a diameter of about 0.06 AU. Considering 1 MC and "a" CL in 2008 we estimate statistically that the number of transients contributing to the result in 2008 to be:

$$\pi\left(2-1/4\right)/\left(\pi/4\right)$$

for MCs, when adding CLs the number climbs to ~15. However, we must distinguish the impact on the CODET modeled temperature and density of the K-corona to be different, since in their majority the CL are smaller structures than the MCs. In this way we reach a total of large de-connections from the Sun with different properties with respect to its quiescent features per day, described here as about:

$$2(\#MC)$$

where we purposely try to overestimate their impact by considering that they displace slowly and expand more quickly to cover about 1/3 of the solar disk for 1/3 of the day, with their impact on the analysis with the CODET model per day to be about:

$$2\ (\#MC/y)/2\ 1/3\pi/\ (1/2\ 2\pi)\ 1/3d/d = 7/365d(1/3)^2 < 1\%$$

of the solar radiance in 2008, when only one MC and no CL were observed, see Wu and Lepping, 2014. Our estimate is based on the same amount of MC and CL generated for that year which is larger than the specific interval of our study, which is focused on the last 2/3 part of 2008. Their contribution would amount to a systematic error in relation to the presence of intervals, most likely of depletion in the temperature, but also affecting the e-count (density number) of electrons of about Area in units of MCs*#MC&CL*duration observation/Area Corona*total time observation.